Enhanced BNC Approach for Non-Circular Signals Direction Finding with Sparse Array in the Scenario of Impulsive Noise

Xudong Dong, Meng Sun, Jun Zhao, Xiaofei Zhang, and Yide Wang

***Abstract*—Sparse array is popular in the field of array signal processing. However, in direction of arrival (DOA) estimation, most research on sparse array assumes Gaussian noise, resulting in model mismatch in the practical scenarios of impulsive noise. We investigate the estimation performance of the bounded non-linear covariance (BNC) matrix based methods, which can be used to replace the original data covariance matrix of the received signal and achieve good robustness to the impulsive interference. We propose an enhanced BNC (EBNC) matrix with non-circular signal for nested array in the scenario of impulsive noise. The proposed EBNC matrix can fight against the impulsive noise outliers and its boundedness and convergence are shown. The proposed method's performance is assessed with simulations. Simulation results indicate that the proposed method provides better performance in DOA estimation than the classical BNC, correntropy-based covariance matrix and Gaussian covariance based methods, especially in highly impulsive noise scenario.**

***Index Terms*—Sparse array, DOA estimation, non-circular signal, bounded non-linear covariance (BNC), impulsive noise.**

I. Introduction

DIRECTION of arrival (DOA) estimation is an essential research topic in array signal processing which has been extensively applied to radar, sonar, wireless communication and electronic reconnaissance [1]. The conventional subspace-based DOA estimation methods, like MUSIC [2] and ESPRIT [3], allow estimation of $N-1$ incoherent narrowband sources by utilizing a uniform linear array (ULA) equipped with N sensors. However, as the number of sources outnumbers the sensors, DOA estimation becomes an underdetermined estimation problem, which is of increasing concern.

To address the above issues, several sparse array-based approaches, such as minimum redundant array (MRA) [4], co-prime array (CA) [5]–[8], and nested array (NA) [9]–[12], are proposed to increase the number of detectable sources and improve the estimation accuracy. Specifically, MRA maximizes the number of virtual sensors in a difference co-array, but there is no closed expression for the array configuration. By consisting of two parallel ULAs, the co-prime array [5] increases the number of detectable sources. For a higher degrees of freedom (DOFs) and better estimation accuracy, series of CA-based array configurations are proposed [6]–[8]. However, the difference co-array in the co-prime array virtualization method results in the absence of virtual sensors (i.e., holes), which degrades the estimation performance. Comparatively, the nested array [9] consisting of a dense and a sparse ULA, whose virtual difference array has no holes. A nested array equipped with N sensors is then capable of achieving $O(N^2)$ DOFs. Compared to the conventional nested array, the proposed super nested array and augmented nested array further improve the DOFs by modifying the dense subarrays.

Nevertheless, the above mentioned methods only notice the difference co-array of sparse arrays without the contribution of sum co-array. Exploiting the non-circular property [13]–[23] of the signal, combined with the sparse array virtualization technique [16]–[23] can produce sum-difference co-arrays, which greatly improve the degrees of freedom and array aperture, thus enhancing the performance of DOA estimation methods based on circular signals. However, the approaches as described above assume that the noise follows a Gaussian distribution. Impulsive noise is generally defined in literatures as external noise to the system that occupies the time domain for a sufficiently short time relative to the block transmission symbol duration and presents impulsive and time-domain sparse characteristics [24], [25]. Impulsive noise has a wide range of causes, usually including astronomical noise generated in the atmospheric space, sparking noise produced by vehicles, electrical and industrial equipment operation noise. Moreover, the statistical distribution of impulsive noise is non-Gaussian distribution, such as α-stable distribution, Gaussian mixture model (GMM), compound Gaussian model (CGM) [26] and generalized Gaussian distribution (GGD) [27]. Among them, elaborate that the α-stable distribution is the most appropriate to describe impulsive noise [28], [29]. To combat impulsive noise, the correlation entropy property [30]–[34], sparse representation [35]–[38], sparse Bayesian learning (SBL, [26], [39], [40]) and l_p-MUSIC based algorithms [27] are already employed for DOA estimation. By exploiting the non-circular characteristics of the signal, [41] proposes an extended MUSIC algorithm based on the covariance property, which improves the performance of the MUSIC method for circular signals. Furthermore, the bounded nonlinear covariance (BNC) matrix [42], [43] based methods are proposed, where the BNC matrix is applied to suppress the outliers of the impulse noise. Nevertheless, only traditional ULAs are considered in the above methods, and the introduction of the sparse array technique is open to further discussion.

Recently, the sparse array techniques are also extended to the impulsive noise scenario [44], [45]. In [44], the Toeplitz phased fractional low-order moment method based on co-prime array is proposed and on this basis, a non-circular

(Corresponding author: Meng Sun.)

X. Dong, X. Zhang and M. Sun are with the Nanjing University of Aeronautics and Astronautics, Nanjing 210000, China(e-mail: nanhangdxd@nuaa.edu.cn; zhangxiaofei@nuaa.edu.cn; mengsun@nuaa.edu.cn).

Yide Wang is with the IETR, University of Nantes, 44306 Nantes, France (e-mail: yide.wang@univ-nantes.fr).

J. Zhao is with the Tongji University, Shanghai 201800, China (e-mail: jun325709@163.com).

signal version of this method is proposed in [45], which obtains better algorithmic performance than [44]. However, the resistance of the PFLOM method to impulsive interference is limited. Inspired by the concept of BNC [43] matrix, this paper proposes an enhanced BNC (EBNC) method for non-circular signals with sparse array in the scenario of impulsive noise, the core idea is to replace the data covariance matrix of the received signal with the EBNC matrix. Since the techniques of sparse array are all interoperable and the difference lies in their continuous ULA of the sum or difference co-array, in this paper, we take the nested array as an example. Furthermore, the reduced dimensional MUSIC (RD-MUSIC) method is applied to DOA estimation for avoiding the computational complexity of two-dimensional search. Simulation results indicate that the proposed method has a stronger resistance to impulsive noise compared with exiting methods. In the following, the main contributions of this paper are ummerized as:

- We extend the concept of the sparse array-based technique to the impulsive noise scenario, which provides a new perspective for this technique.
- We propose an enhanced bounded non-linear function (EBNF) and also give an algorithmic concept of an enhanced BNC (EBNC) matrix based on EBNF to combat the impulsive noise. In addition, the RD-MUSIC method with nested array is employed to perform DOA estimation, reducing the computational complexity while improving the estimation accuracy.
- The proposed method is also extensible to other sparse array geometries, such as co-prime arrays, super nested arrays, etc.

The rest of this paper is structured as follows: Section II presents some backgrounds, including the data model with nested array and BNC matrix. The proposed EBNC based method in presence of impulsive noise are described in section III. Section IV and V provide the numerical result and conclusion, respectively.

II. Backgrounds

A. Data model

Co-prime and nested arrays [5], [9] are sparse arrays of simple geometries with closed-form expression, where the nested array consists of a dense ULA with sensor spacing d_0 and a sparse ULA with sensor separation $(N_1+1)d_0$. The sensor locations of the nested array are given by [9]:

$$\begin{aligned}\mathcal{L} &= \{md_0 \,|m = 1, \cdots, N_1\} \\ &\cup \{n\left(N_1+1\right)d_0 \,|n = 1, \cdots, N_2\},\end{aligned} \tag{1}$$

where N_1 and N_2 are positive integers. Let $\mathcal{L} = \{l_1, l_2, \cdots, l_P\}$, and an integer set $\bar{\mathcal{L}} = \left\{\bar{l}_1, \bar{l}_2, \cdots, \bar{l}_P\right\}$ is also available, where $\bar{l}_p = l_p/d_0$ for $p = 1, \cdots, P$.

We consider K far field incoherent narrowband signals from $\theta_1, \cdots, \theta_K$, impinging on a nested array, the array output is

$$\mathbf{x}\left(t\right) = \mathbf{A}\mathbf{s}\left(t\right) + \mathbf{n}\left(t\right), t = 1, \cdots, T, \tag{2}$$

where $\mathbf{A} = \left[\mathbf{a}\left(\omega_1\right), \cdots, \mathbf{a}\left(\omega_k\right), \cdots \mathbf{a}\left(\omega_K\right)\right]$ is the directional matrix and $\mathbf{s}(t) = \left[s_1(t), \cdots, s_k(t), \cdots s_K(t)\right]^T$ is the source signal vector, T denotes the number of snapshots and $(\cdot)^T$ is the transpose, $\mathbf{n}\left(t\right) = \left[n_1\left(t\right), \cdots, n_P\left(t\right)\right]^T$ is an impulsive noise term and the direction vector $\mathbf{a}\left(\omega_k\right)$ is

$$\mathbf{a}\left(\omega_k\right) = \left[e^{-j\bar{l}_1\omega_k}, e^{-j\bar{l}_2\omega_k}, \cdots, e^{-j\bar{l}_P\omega_k}\right]^T, \tag{3}$$

where $\omega_k = (2\pi d_0 \sin\theta_k)/\lambda$ with λ the carrier wavelength. In this paper, we adopt the following assumptions:

A1: The signal $\mathbf{s}(t) = \mathbf{\Phi}\mathbf{s}_0\left(t\right)$ in Eq. (2) are strict non-circular signal (for example, binary phase shift keying (BPSK) and amplitude modulation (AM) signals). $\mathbf{\Phi} = diag\left\{e^{-j\varphi_1}, \cdots, e^{-j\varphi_K}\right\}$ with φ_k the non-circular phase, $\mathbf{s}_0\left(t\right) = \left[s_{01}(t), \cdots, s_{0k}(t), \cdots, s_{0K}(t)\right]^T$.

A2: In practical scenarios, the noise consists of irregular pulses or spikes of short duration and large amplitude, where the traditional second-order statistics are no longer applicable. $\mathbf{n}\left(t\right)$ is a sequence of independent identically distributed (IID). isotropic complex symmetric α stable ($S\alpha S$) [24] random variables with characteristic exponent $0 < \alpha \leqslant 2$, which is independent of the signals. And the complex $S\alpha S$ process can be expressed as

$$n_p\left(t\right) \sim \mathcal{CS}\left(\cdot\,|\alpha, \gamma\right), p = 1, \cdots, P, \tag{4}$$

where $\mathcal{CS}\left(\cdot\,|\alpha, \gamma\right)$ is the isotropic complex $S\alpha S$ process with characteristic exponent α and dispersion parameter γ. The probability density function (PDF) of complex $S\alpha S$ process hasn't closed-form expression when $\alpha \neq 1$ and $\alpha \neq 2$, but the characteristic function can be given as

$$\phi(t) = \exp\left(-\gamma^{\alpha}|t|^{\alpha}\right),$$

when $\alpha = 2$, it becomes a Gaussian distribution and it turns into a Cauchy distribution at $\alpha = 1$.

A3: By exploiting the non-circular property of the signals, the Eq. (2) can be extended as:

$$\mathbf{y}\left(t\right) = \begin{bmatrix}\mathbf{x}\left(t\right) \\ \mathbf{x}^*\left(t\right)\end{bmatrix} = \hat{\mathbf{A}}\mathbf{s}_0\left(t\right) + \begin{bmatrix}\mathbf{n}\left(t\right) \\ \mathbf{n}^*\left(t\right)\end{bmatrix}, \tag{5}$$

the new directional matrix $\hat{\mathbf{A}}$ can be obtained by

$$\hat{\mathbf{A}} = \begin{bmatrix}\mathbf{A}\mathbf{\Phi} \\ \mathbf{A}^*\mathbf{\Phi}^*\end{bmatrix} = \left[\hat{\mathbf{a}}\left(\theta_1, \varphi_1\right), \cdots, \hat{\mathbf{a}}\left(\theta_K, \varphi_K\right)\right], \tag{6}$$

$$\hat{\mathbf{a}}\left(\theta_k, \varphi_k\right) = \begin{bmatrix}\mathbf{a}\left(\theta_k\right)e^{-j\varphi_k} \\ \mathbf{a}^*\left(\theta_k\right)e^{j\varphi_k}\end{bmatrix}, \tag{7}$$

where $(\cdot)^*$ is the conjugate operation.

B. Bounded non-linear covariance (BNC) matrix

1) Bounded non-linear function (BNF): To effectively fight against the impulsive noise, the bounded nonlinear function (BNF) proposed in [43] can be expressed as:

$$g\left(x\right) = \begin{cases} f\left(x\right) & x \geqslant x_0 \\ l\left(x\right) & x \in \left(-x_0, x_0\right) \\ f\left(x\right) & x \leqslant -x_0 \end{cases}, \tag{8}$$

where $f(x)$ and $l(x)$ are odd functions. Meanwhile, $l\left(x\right) \approx x$ and $f(x)$ satisfies $max|f(x)| \leqslant f_0$, where $f_0 > x_0 > 0$ is a positive constant.

Obviously, $g(x)$ is a bounded odd function. Therefore it is nonlinear outside the interval $(-x_0, x_0)$, while $g(x) =$

$l(x) \approx x$ is approximately considered as linear in the interval $(-x_0, x_0)$. It can represent the original value of the variable x by linear transformation and suppress the outliers of the variable x by nonlinear boundedness.

The Cauchy score function is a typical BNF, which can be expressed as

$$score\left(x\right) = \frac{2\lambda_4 x}{1+(\lambda_3 x)^2}, \tag{9}$$

where λ_3 and λ_4 are tunable parameters for adjusting the almost linear region of the signal. A Taylor's expansion of $score(x)$ at $x = 0$ yields

$$score\left(x\right) = 2\lambda_4 x + o(x^2). \tag{10}$$

According to (10), we know that $score(x) = x$ when $\lambda_4 = 0.5$ within the range around $x = 0$.

2) Bounded non-linear covariance (BNC) matrix: When array signal processing is involved, the (i,j)-th element of the BNC matrix $\mathbf{R}^{\text{BNC}}$ of the nested array output $\mathbf{y}(t)$ is defined as

$$r_{ij}^{\text{BNC}} = \text{BNC}(y_i(t), y_j(t)) = \mathbb{E}\left(g\left(y_i(t)\right) g^H\left(y_j(t)\right)\right), \tag{11}$$

where $(\cdot)^H$ is the conjugate transpose and $y_i(t)$ denotes the i-th element of $\mathbf{y}\left(t\right)$.

Remark 1: Note that x in Eq. (8) is a real number, but in array signal processing, Eq. (5) belongs to the complex domain. Therefore, we use a real-virtual partial calculation in the calculation of the BNC matrix in Eq. (11), i.e. $g\left(y_i(t)\right) = g\left(real\left(y_i(t)\right)\right) + j \times g\left(imag\left(y_i(t)\right)\right)$. Furthermore, according to the properties of the odd function $g(x)$, we have

$$\begin{aligned} & g\left(y_i^*(t)\right) = g\left(real\left(y_i^*(t)\right)\right) + j \times g\left(imag\left(y_i^*(t)\right)\right) \\ & = g\left(real\left(y_i(t)\right)\right) - j \times g\left(imag\left(y_i(t)\right)\right) \\ & = g^*\left(y_i(t)\right) \\ & = g^H\left(y_i(t)\right), \end{aligned}$$

where $real(c)$ and $imag(c)$ are the real and imaginary parts of the complex number c, respectively.

III. Proposed Enhanced BNC Based Method in Presence of Impulsive Noise

A. Construction of BNC matrix

In DOA estimation, the mean value of the signal is generally zero. The signal is more resistant to impulsive noise interference in the range around zero mean, which can achieve a better DOA estimation. Based on the suppression ability and boundedness of BNC matrix, we propose a new DOA estimation method, called as NA-NC-BNC, and the BNC matrix for non-circular signals can be expressed as

$$\mathbf{R}^{\text{BNC}} = \text{BNC}\left(\mathbf{y}\left(t\right), \mathbf{y}\left(t\right)\right) = \begin{bmatrix} \mathbf{R}_{\text{BNC}}^1 & \mathbf{R}_{\text{BNC}}^2 \\ \mathbf{R}_{\text{BNC}}^3 & \mathbf{R}_{\text{BNC}}^4 \end{bmatrix}, \tag{12}$$

where the (i,j)-th elements of these four sub-matrices are

$$\begin{aligned} r_{ij}^1 &= \text{BNC}\left(x_i\left(t\right), x_j\left(t\right)\right) = \mathbb{E}\left(g\left(x_i(t)\right) g^H\left(x_j(t)\right)\right) \\ r_{ij}^2 &= \text{BNC}\left(x_i\left(t\right), x_j^*\left(t\right)\right) = \mathbb{E}\left(g\left(x_i(t)\right) g^H\left(x_j^*(t)\right)\right) \\ r_{ij}^3 &= \text{BNC}\left(x_i^*\left(t\right), x_j\left(t\right)\right) = \mathbb{E}\left(g\left(x_i^*(t)\right) g^H\left(x_j(t)\right)\right) \\ r_{ij}^4 &= \text{BNC}\left(x_i^*\left(t\right), x_j^*\left(t\right)\right) = \mathbb{E}\left(g\left(x_i^*(t)\right) g^H\left(x_j^*(t)\right)\right) \end{aligned} \tag{13}$$

From [43], the BNC matrix (12) can be also expressed as

$$\mathbf{R}^{\text{BNC}} = \hat{\mathbf{A}} \mathbf{R}_{\mathbf{s}_0}^{\text{BNC}} \hat{\mathbf{A}}^H + \mathbf{\Gamma}, \tag{14}$$

where $\mathbf{R}_{\mathbf{s}0}^{\text{BNC}} = diag\left(\kappa_{01}, \cdots, \kappa_{0k}, \cdots, \kappa_{0K}\right)$ is a diagonal matrix of signal $\mathbf{s}_0(t)$, in which $\kappa_{0k} = \text{BNC}\left(s_{0k}\left(t\right), s_{0k}\left(t\right)\right)$. $\mathbf{\Gamma} = \sigma_n^2 \mathbf{I}_{2P}$, σ_n^2 is the approximate variance of impulsive noise and $\mathbf{I}_{2P}$ is the identity matrix of dimensions $2P$. Appendix A gives the proof of Eq. (14).

B. Construction of enhanced BNC matrix

Unfortunately, the performance of BNC method degrades at low GSNR and highly impulsive scenarios. To address this issue, we propose an enhanced bounded nonlinear covariance (EBNC) matrix, which will have an improved resistance to impulsive interference in the highly impulsive scenarios.

Definition 1: In this paper, the enhanced bounded nonlinear function (EBNF) is defined as

$$G(x) = \begin{cases} f\left(|x|^{p-2} \times x\right) & x \geqslant x_0 \\ l\left(|x|^{p-2} \times x\right) & (-x_0, 0) \cup (0, x_0) \\ f\left(|x|^{p-2} \times x\right) & x \leqslant -x_0 \end{cases}, \tag{15}$$

where $0 < p \leqslant 2$ is a order moment constant. It can be seen that $|x|^{p-2}$ is an bounded even function, so $G(x)$ still satisfies the boundedness condition. Obviously, EBNF degenerates to BNF when $p = 2$.

Definition 2: If X and Y are two real random variables, the EBNC can be denoted as r^{EBNC}, i.e.

$$r^{\text{EBNC}}(X, Y) = \mathbb{E}\left[G(X) G^H(Y)\right]. \tag{16}$$

Based on the definitions of EBNF and EBNC, the EBNC matrix of stochastic vector $\mathbf{X} = [X_1, X_2, \cdots, X_P]^T$ is denoted as $\mathbf{R}^{\text{EBNC}}$ and its (i,j)-th element can be defined as

$$r_{ij}^{\text{EBNC}} = \mathbb{E}\left\{G\left(X_i\right) G^H\left(X_j\right)\right\}. \tag{17}$$

The $\mathbf{R}^{\text{EBNC}}$ can be regarded as an approximation of the traditional second-order covariance matrix, while the boundedness and nonlinearity of $\mathbf{R}^{\text{EBNC}}$ can also suppress the large outliers of impulsive noise. Appendix B and C provide the boundedness proof of EBNF and the convergence of EBNC, respectively. We propose the NA-NC-EBNC method by replacing the EBNC matrix with the BNC matrix, and the choice of p is given in section IV.

Remark 2: We multiply the BNF by $|x|^{p-2}$, where $0 < p \leqslant 2$. As the absolute value of x becomes larger, the $|x|^{p-2}$ becomes smaller, which corresponds to a secondary suppression of impulsive noise interference, resulting in the EBNC matrix $\mathbf{R}^{\text{EBNC}}$ based on the array output $\mathbf{y}(t)$ and its (i,j)-th element can be expressed as

$$r_{ij}^{\text{EBNC}} = \mathbb{E}\left(G\left(y_i'(t)\right) G^H\left(y_j'(t)\right)\right) \tag{18}$$

where $G\left(y_i'(t)\right) = G\left(real\left(y_i'(t)\right)\right) + j \times G\left(imag\left(y_i'(t)\right)\right)$ and $y_i'(t) = |y_i'(t)|^{p-2} y_i'(t)$.

In the following subsection, the index BNC in $\mathbf{R}^{\text{BNC}}$, the index EBNC in $\mathbf{R}^{\text{EBNC}}$, are dropped for notational convenience.

C. Nested array approach

1) Sum co-array and difference co-array: According to [20], the virtual sensors set of difference co-array and sum co-array can be denoted as

$$\mathcal{D}=\left\{\bar{l}_i-\bar{l}_j\middle|\,\bar{l}_i,\bar{l}_j\in\bar{\mathcal{L}}\right\},\tag{19}$$

and

$$\begin{aligned}\mathcal{S}&=\mathcal{S}^+\cup\mathcal{S}^-\\ \mathcal{S}^+&=\left\{\bar{l}_i+\bar{l}_j\right\}\\ \mathcal{S}^-&=\left\{-\bar{l}_i-\bar{l}_j\right\}\end{aligned}.\tag{20}$$

Fig. 1 illustrates the co-array of nested arrays, where $N_1=N_2=3$. and (a) is a difference co-array with sensors continuously located in $\langle-11,11\rangle d_0$, (b) is a positive sum co-array with successive positions of $\langle 0,14\rangle d_0$ and (c) is the negative sum co-array and its consecutive locations are $\langle-14,0\rangle d_0$. According to [9], when N_1 and N_2 are given, the consecutive positions of the difference co-array are $\langle-M_1,M_1\rangle d_0$, and the sum co-arrays are continuously distributed on $\langle-M_2,0\rangle d_0$ and $\langle 0,M_2\rangle d_0$, respectively, where $M_1=N_1N_2+N_2-1$ and $M_2=N_1N_2+N_1+N_2-1$.

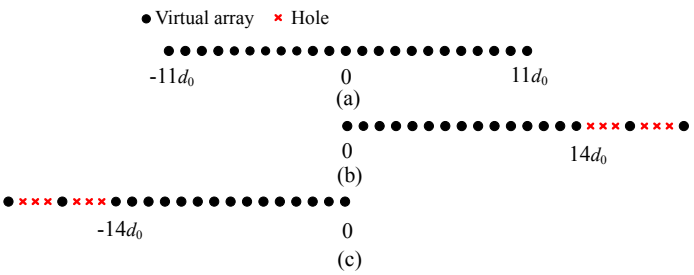

Fig. 1: co-array of nested arrays with $N_1=N_2=3$. (a) difference co-array $\mathcal{D}$, (b) positive sum co-array $\mathcal{S}^+$, (c) negative sum co-array $\mathcal{S}^-$.

2) Vectorization: By vectorizing the equivalent covariance matrix (include $\mathbf{R}^{\mathrm{BNC}}$ and $\mathbf{R}^{\mathrm{EBNC}}$ matrices, we take $\mathbf{R}^{\mathrm{BNC}}$ as an example), then we have

$$\mathbf{z}=vec\left(\mathbf{R}\right)=\left(\hat{\mathbf{A}}^*\odot\hat{\mathbf{A}}\right)\mathbf{p}+vec\left(\mathbf{\Gamma}\right),\tag{21}$$

where $\mathbf{p}$ is a vector of $\mathbf{R}_{\mathbf{s}_0}^{\mathrm{BNC}}$'s diagonal elements, and the k-th vector of $\mathbf{H}=\left(\hat{\mathbf{A}}^*\odot\hat{\mathbf{A}}\right)=\left[\mathbf{h}\left(\theta_1,\varphi_1\right),\cdots,\mathbf{h}\left(\theta_K,\varphi_K\right)\right]$ is [19] [20]

$$\begin{aligned}\mathbf{h}\left(\theta_k,\varphi_k\right)&=\hat{\mathbf{a}}^*\left(\theta_k,\varphi_k\right)\otimes\hat{\mathbf{a}}\left(\theta_k,\varphi_k\right)\\&=\begin{bmatrix}\mathbf{a}^*\left(\theta_k\right)e^{j\varphi_k}\\ \mathbf{a}\left(\theta_k\right)e^{-j\varphi_k}\end{bmatrix}\otimes\begin{bmatrix}\mathbf{a}\left(\theta_k\right)e^{-j\varphi_k}\\ \mathbf{a}^*\left(\theta_k\right)e^{j\varphi_k}\end{bmatrix},\end{aligned}\tag{22}$$

where $\otimes$ and $\odot$ denote Kronecker and Khatri-Rao products, respectively. Multiplying Eq. (22) by the row transformation matrix $\mathbf{J}$, we can obtain

$$\begin{aligned}\tilde{\mathbf{h}}\left(\theta_k,\varphi_k\right)&=\mathbf{J}\mathbf{h}\left(\theta_k,\varphi_k\right)\\&=\begin{bmatrix}\mathbf{a}^*\left(\theta_k\right)\otimes\mathbf{a}\left(\theta_k\right)\\ \mathbf{a}^*\left(\theta_k\right)\otimes\mathbf{a}^*\left(\theta_k\right)e^{2j\varphi_k}\\ \mathbf{a}\left(\theta_k\right)\otimes\mathbf{a}\left(\theta_k\right)e^{-2j\varphi_k}\\ \mathbf{a}\left(\theta_k\right)\otimes\mathbf{a}^*\left(\theta_k\right)\end{bmatrix},\end{aligned}\tag{23}$$

with

$$\mathbf{J}=\begin{bmatrix}\begin{bmatrix}\mathbf{J}_1\\ \mathbf{J}_2\end{bmatrix} & \mathbf{0}_{2P^2}\\ \mathbf{0}_{2P^2} & \begin{bmatrix}\mathbf{J}_1\\ \mathbf{J}_2\end{bmatrix}\end{bmatrix}\in\mathbb{R}^{4P^2\times 4P^2},$$

$$\mathbf{J}_1=\mathbf{I}_P\otimes\begin{bmatrix}\mathbf{I}_P & \mathbf{0}_P\end{bmatrix}\in\mathbb{R}^{P^2\times 2P^2},$$

$$\mathbf{J}_2=\mathbf{I}_P\otimes\begin{bmatrix}\mathbf{0}_P & \mathbf{I}_P\end{bmatrix}\in\mathbb{R}^{P^2\times 2P^2},$$

where $\mathbf{0}_P$ and $\mathbf{I}_P$ are the all-zero matrix and identity matrix of dimension $P\times P$, respectively. Then we can obtain

$$\tilde{\mathbf{z}}=\mathbf{J}\mathbf{z}=\tilde{\mathbf{H}}\mathbf{p}+\mathbf{J}vec(\mathbf{\Gamma}),\tag{24}$$

with $\tilde{\mathbf{H}}=[\tilde{\mathbf{h}}\left(\theta_1,\varphi_1\right),\cdots,\tilde{\mathbf{h}}\left(\theta_K,\varphi_K\right)]$. According to (24), we can divide $\tilde{\mathbf{H}}$ into four parts $\mathcal{H}_1,\mathcal{H}_2,\mathcal{H}_3,\mathcal{H}_4\in\mathbb{C}^{P^2\times K}$, i.e., $\tilde{\mathbf{H}}=[\mathcal{H}_1;\mathcal{H}_2;\mathcal{H}_3;\mathcal{H}_4]$, and

$$\begin{aligned}\mathcal{H}_1&=\left[\mathbf{a}^*\left(\theta_1\right)\otimes\mathbf{a}\left(\theta_1\right),\cdots,\mathbf{a}^*\left(\theta_K\right)\otimes\mathbf{a}\left(\theta_K\right)\right],\\ \mathcal{H}_2&=\left[\mathbf{a}^*\left(\theta_1\right)\otimes\mathbf{a}^*\left(\theta_1\right),\cdots,\mathbf{a}^*\left(\theta_K\right)\otimes\mathbf{a}^*\left(\theta_K\right)\right]\mathbf{\Phi}^{-2},\\ \mathcal{H}_3&=\left[\mathbf{a}\left(\theta_1\right)\otimes\mathbf{a}\left(\theta_1\right),\cdots,\mathbf{a}\left(\theta_K\right)\otimes\mathbf{a}\left(\theta_K\right)\right]\mathbf{\Phi}^{2},\\ \mathcal{H}_4&=\left(\mathbf{a}\left(\theta_1\right)\otimes\mathbf{a}^*\left(\theta_1\right),\cdots,\mathbf{a}\left(\theta_K\right)\otimes\mathbf{a}^*\left(\theta_K\right)\right).\end{aligned}$$

In order to remove the redundant items and select the virtual continuous ULA information in (24), we introduce a selection matrix as follows

$$\mathbf{F}_{1,(l_{\mathcal{D}}+M_1+1,i+(j-1)P)}=\begin{cases}\frac{1}{\omega(l_{\mathcal{D}})} & l_{\mathcal{D}}=l_i-l_j,\\ 0 & \text{otherwise},\end{cases}\tag{25}$$

$$l_{\mathcal{D}}=-M_1,\cdots,0,\cdots,M_1,\,and\,\mathbf{F}_1\in\mathbb{C}^{(2M_1+1)\times P^2},$$

$$\mathbf{F}_{2,(l_{\mathcal{S}}^-+M_2+1,i+(j-1)P)}=\begin{cases}\frac{1}{\omega(l_{\mathcal{S}}^-)} & l_{\mathcal{S}}^-=-l_i-l_j\\ 0 & \text{otherwise},\end{cases}\tag{26}$$

$$l_{\mathcal{S}}^-=-M_2,\cdots,-1,0,\,and\,\mathbf{F}_2\in\mathbb{C}^{(M_2+1)\times P^2},$$

$$\mathbf{F}_{3,(l_{\mathcal{S}}^++1,i+(j-1)P)}=\begin{cases}\frac{1}{\omega(l_{\mathcal{S}}^+)} & l_{\mathcal{S}}^+=l_i+l_j\\ 0 & \text{otherwise},\end{cases}\tag{27}$$

$$l_{\mathcal{S}}^+=0,1,\cdots,M_2,\,and\,\mathbf{F}_3\in\mathbb{C}^{(M_2+1)\times P^2},$$

$$\mathbf{F}_{4,(l_{\mathcal{D}}+M_1+1,i+(j-1)P)}=\begin{cases}\frac{1}{\omega(l_{\mathcal{D}})} & l_{\mathcal{D}}=l_j-l_i\\ 0 & \text{otherwise},\end{cases}\tag{28}$$

$$l_{\mathcal{D}}=-M_1,\cdots,0,\cdots,M_1,\,and\,\mathbf{F}_4\in\mathbb{C}^{(2M_1+1)\times P^2},$$

where $\mathbf{F}_{i,(s,t)}$ is the (s,t)-th element of the i-th selection matrix $\mathbf{F}_i,i=1,2,3,4$, $\omega(m)$ stands for the cardinality of m defined as

$$\omega(m)=\left|\mathbb{D}\left(m\right)\right|,\left|\mathbb{S}^+\left(m\right)\right|\text{ or }\left|\mathbb{S}^-\left(m\right)\right|$$

with

$$\begin{aligned}\mathbb{D}\left(m\right)&=\left\{\left(\bar{l}_i,\bar{l}_j\right)\middle|\,\bar{l}_i-\bar{l}_j=m,\bar{l}_i,\bar{l}_j\in\bar{\mathcal{L}}\right\},\\ \mathbb{S}^+\left(m\right)&=\left\{\left(\bar{l}_i,\bar{l}_j\right)\middle|\,\bar{l}_i+\bar{l}_j=m,\bar{l}_i,\bar{l}_j\in\bar{\mathcal{L}}\right\},\\ \mathbb{S}^-\left(m\right)&=\left\{\left(\bar{l}_i,\bar{l}_j\right)\middle|\,-\bar{l}_i-\bar{l}_j=m,\bar{l}_i,\bar{l}_j\in\bar{\mathcal{L}}\right\},\end{aligned}$$

where $|\mathbb{X}|$ denotes the cardinality of a set $\mathbb{X}$.

Then we have

$$\begin{aligned}\tilde{\mathbf{z}}_{\text{ULA}} &= \mathbf{F}\tilde{\mathbf{z}} \\ &= blkdiag\left\{\mathbf{F}_1,\mathbf{F}_2,\mathbf{F}_3,\mathbf{F}_4\right\}\tilde{\mathbf{z}} \\ &= \left[\mathbf{F}_1\mathcal{H}_1;\mathbf{F}_2\mathcal{H}_2;\mathbf{F}_3\mathcal{H}_3;\mathbf{F}_4\mathcal{H}_4\right]\mathbf{p}+\mathbf{F}\mathbf{J}vec\left(\mathbf{\Gamma}\right) \\ &= \begin{bmatrix}\tilde{\mathbf{H}}_1\\ \tilde{\mathbf{H}}_2\\ \tilde{\mathbf{H}}_3\\ \tilde{\mathbf{H}}_4\end{bmatrix}\mathbf{p}+\begin{bmatrix}\gamma_1\\ \gamma_2\\ \gamma_3\\ \gamma_4\end{bmatrix} = \begin{bmatrix}\tilde{\mathbf{z}}_1\\ \tilde{\mathbf{z}}_2\\ \tilde{\mathbf{z}}_3\\ \tilde{\mathbf{z}}_4\end{bmatrix}\end{aligned} \tag{29}$$

with

$$\tilde{\mathbf{H}}_1 = \left[\tilde{\mathbf{h}}_1\left(\theta_1\right),\cdots,\tilde{\mathbf{h}}_1\left(\theta_K\right)\right] \in \mathbb{C}^{(2M_1+1)\times K} \tag{29a}$$

$$\tilde{\mathbf{H}}_2 = \left[\tilde{\mathbf{h}}_2\left(\theta_1,\varphi_1\right),\cdots,\tilde{\mathbf{h}}_2\left(\theta_K,\varphi_K\right)\right] \in \mathbb{C}^{(M_2+1)\times K} \tag{29b}$$

$$\tilde{\mathbf{H}}_3 = \left[\tilde{\mathbf{h}}_3\left(\theta_1,\varphi_1\right),\cdots,\tilde{\mathbf{h}}_3\left(\theta_K,\varphi_K\right)\right] \in \mathbb{C}^{(M_2+1)\times K} \tag{29c}$$

$$\tilde{\mathbf{H}}_4 = \left[\tilde{\mathbf{h}}_4\left(\theta_1\right),\cdots,\tilde{\mathbf{h}}_4\left(\theta_K\right)\right] \in \mathbb{C}^{(2M_1+1)\times K} \tag{29d}$$

$$\tilde{\mathbf{h}}_1\left(\theta_k\right) = \left[e^{j\pi M_1\sin\theta_k},\cdots 1,\cdots,e^{-j\pi M_1\sin\theta_k}\right]^T \tag{29e}$$

$$\tilde{\mathbf{h}}_2\left(\theta_k,\varphi_k\right) = e^{2j\varphi_k}\left[e^{j\pi M_2\sin\theta_k},\cdots,1\right]^T \tag{29f}$$

$$\tilde{\mathbf{h}}_3\left(\theta_k,\varphi_k\right) = e^{-2j\varphi_k}\left[1,\cdots,e^{-j\pi M_2\sin\theta_k}\right]^T \tag{29g}$$

$$\tilde{\mathbf{h}}_4\left(\theta_k\right) = \left[e^{j\pi M_1\sin\theta_k},\cdots 1,\cdots,e^{-j\pi M_1\sin\theta_k}\right]^T, \tag{29h}$$

where $blkdiag\{\cdot\}$ is a matrix block diagonal operation. γ_2,γ_3 and γ_1,γ_4 are the noise vector corresponding to the sum co-array and difference co-array, respectively.

D. Spatial smoothing technique for SD co-array

Actually, by calculating (25)-(28), we find that $\tilde{\mathbf{z}}_1$ and $\tilde{\mathbf{z}}_4$ incorporate the same difference co-array information. Since $\tilde{\mathbf{z}}_1$, $\tilde{\mathbf{z}}_2$ and $\tilde{\mathbf{z}}_3$ is a single snapshot vector, the spatial smoothing (SS) algorithm should be used for decoherence [7]. We separate $\tilde{\mathbf{z}}_1$ into M_1+1 overlapping subarrays, $\tilde{\mathbf{z}}_{D,m}, m=1,\cdots,M_1+1$, each with M_1+1 virtual array elements, i.e.,

$$\tilde{\mathbf{Z}}_D = \left[\tilde{\mathbf{z}}_{D,1},\cdots,\tilde{\mathbf{z}}_{D,M_1+1}\right] \tag{30}$$

with

$$\begin{aligned}\tilde{\mathbf{z}}_{D,m} &= \tilde{\mathbf{z}}_1\left(M_1+2-m:2M_1+2-m,:\right) \\ &= \mathbf{H}_D\mathbf{\Psi}^{m-1}\mathbf{p}+\gamma_{D,m}, m=1,\cdots,M_1+1\end{aligned} \tag{30a}$$

$$\mathbf{H}_D = \left[\mathbf{h}_D\left(\theta_1\right),\cdots,\mathbf{h}_D\left(\theta_K\right)\right] \tag{30b}$$

$$\mathbf{h}_D\left(\theta_k\right) = \begin{bmatrix}1\\ e^{-j\pi\sin\theta_k}\\ \vdots\\ e^{-jM_1\pi\sin\theta_k}\end{bmatrix} \tag{30c}$$

$$\mathbf{\Psi} = \begin{bmatrix}e^{j\pi\sin\theta_1} & & \\ & \ddots & \\ & & e^{j\pi\sin\theta_K}\end{bmatrix} \tag{30d}$$

$$\gamma_{D,m} = \gamma_1\left(M_1+2-m:2M_1+2-m,:\right), \tag{30e}$$

where $\mathbf{H}_D$ is the directional matrix and $\mathbf{\Psi}$ is a rotation matrix.

Similar to Eq. (30), we also divide $\tilde{\mathbf{z}}_2$ into M_1+1 overlapping subarrays $\tilde{\mathbf{z}}_{S^-,m}, m=1,\cdots,M_1+1$, each with M_2-M_1+1 array elements (actually, $M_2-M_1+1=N_1+1$), i.e.,

$$\tilde{\mathbf{Z}}_{S^-} = \left[\tilde{\mathbf{z}}_{S^-,1},\cdots,\tilde{\mathbf{z}}_{S^-,M_1+1}\right] \tag{31}$$

with

$$\begin{aligned}\tilde{\mathbf{z}}_{S^-,m} &= \tilde{\mathbf{z}}_2\left(M_1+2-m:M_2+2-m,:\right) \\ &= \mathbf{H}_{S^-}\mathbf{\Psi}^{m-1}\mathbf{p}+\gamma_{S^-,m}, m=1,\cdots,M_1+1\end{aligned} \tag{31a}$$

$$\mathbf{H}_{S^-} = \left[\mathbf{h}_{S^-}\left(\theta_1,\varphi_1\right),\cdots,\mathbf{h}_{S^-}\left(\theta_K,\varphi_K\right)\right] \tag{31b}$$

$$\mathbf{h}_{S^-}\left(\theta_k,\varphi_k\right) = \begin{bmatrix}e^{-j(M_1-M_2)\pi\sin\theta_k}e^{2j\varphi_k}\\ \vdots\\ e^{2j\varphi_k}\end{bmatrix} \tag{31c}$$

$$\gamma_{S^-,m} = \gamma_2\left(M_1+2-m:M_2+2-m,:\right). \tag{31d}$$

Also, for the the positive sum co-array information $\tilde{\mathbf{z}}_2$, we have

$$\tilde{\mathbf{Z}}_{S^+} = \left[\tilde{\mathbf{z}}_{S^+,1},\cdots,\tilde{\mathbf{z}}_{S^+,M_1+1}\right] \tag{32}$$

with

$$\begin{aligned}\tilde{\mathbf{z}}_{S^+,m} &= \tilde{\mathbf{z}}_3\left(M_1+2-m:M_2+2-m,:\right) \\ &= \mathbf{H}_{S^+}\mathbf{\Psi}^{m-1}\mathbf{p}+\gamma_{S^+,m}, m=1,\cdots,M_1+1\end{aligned} \tag{32a}$$

$$\mathbf{H}_{S^+} = \left[\mathbf{h}_{S^+}\left(\theta_1,\varphi_1\right),\cdots,\mathbf{h}_{S^+}\left(\theta_K,\varphi_K\right)\right] \tag{32b}$$

$$\mathbf{h}_{S^+}\left(\theta_k,\varphi_k\right) = \begin{bmatrix}e^{-jM_1\pi\sin\theta_k}e^{-2j\varphi_k}\\ e^{-j(M_1+1)\pi\sin\theta_k}e^{-2j\varphi_k}\\ \vdots\\ e^{-jM_2\pi\sin\theta_k}e^{-2j\varphi_k}\end{bmatrix} \tag{32c}$$

$$\gamma_{S^+,m} = \gamma_3\left(M_1+2-m:M_2+2-m,:\right). \tag{32d}$$

According to Eq.(30)-(32), the reconstructed sum-difference (SD) co-arrays spatial smoothing matrix is

$$\begin{aligned}\mathbf{Z} &= \left[\tilde{\mathbf{Z}}_{S^-};\tilde{\mathbf{Z}}_D;\tilde{\mathbf{Z}}_{S^+}\right] \in C^{(2M_2-M_1+3)\times(M_1+1)} \\ &= \left[\mathbf{z}_1,\cdots,\mathbf{z}_m,\cdots,\mathbf{z}_{M_1+1}\right]\end{aligned} \tag{33}$$

$$\mathbf{z}_m = \overleftrightarrow{\mathbf{H}}\mathbf{\Psi}^{m-1}\mathbf{p}+\overleftrightarrow{\gamma}_m, m=1,\cdots,M_1+1 \tag{34}$$

where

$$\overleftrightarrow{\mathbf{H}} = \left[\overleftrightarrow{\mathbf{h}}\left(\theta_1,\varphi_1\right),\cdots,\overleftrightarrow{\mathbf{h}}\left(\theta_K,\varphi_K\right)\right] \tag{35}$$

$$\overleftrightarrow{\mathbf{h}}\left(\theta_k,\varphi_k\right) = \begin{bmatrix}\mathbf{h}_{S^-}\left(\theta_k,\varphi_k\right)\\ \mathbf{h}_D\left(\theta_k\right)\\ \mathbf{h}_{S^+}\left(\theta_k,\varphi_k\right)\end{bmatrix} \tag{36}$$

$$\overleftrightarrow{\gamma}_m = \left[\gamma_{S^-,m};\gamma_{D,m};\gamma_{S^+,m}\right]. \tag{37}$$

Remark 3: Fig. 2 depicts the corresponding spatial smoothing co-array of the nested array, where $N_1=N_2=3$. From Fig. 2, the following conclusions can be drawn: a) The spatial smoothing subarrays of difference set $\mathcal{D}$ with virtual sensor number M_1+1, which corresponds to the directional vector $\mathbf{h}_D\left(\theta_k\right)$. b) The number of virtual array elements of the spatial smoothing subarray of the positive-sum co-array $\mathcal{S}^+$ and the negative-sum co-array $\mathcal{S}^-$ is M_2-M_1+1, corresponding to the directional vectors $\mathbf{h}_{S^+}\left(\theta_k,\varphi_k\right)$ and

$\mathbf{h}_{S^-}(\theta_k,\varphi_k)$, respectively. Notice that the purpose of this smoothing technique is that the smoothed sub-arrays $\tilde{\mathbf{Z}}_{S^-}$, $\tilde{\mathbf{Z}}_D$ and $\tilde{\mathbf{Z}}_{S^+}$ are the same number of columns, so that the matrix (33) can be considered as a received data with multi-snapshot (snapshot of M_1+1).

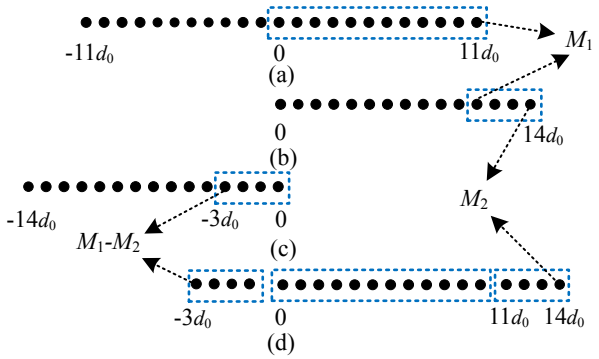

Fig. 2: spatial smoothing co-array with $N_1 = N_2 = 3$. (a) difference co-array, (b) positive sum co-array, (c) negative sum co-array, (d) sum-difference (SD) co-arrays.

E. Reduced-dimension MUSIC method

According to (33), the covariance matrix $\mathbf{R}_Z$ can be expressed as

$$\mathbf{R}_Z = \frac{1}{M_1+1}\mathbf{Z}\mathbf{Z}^H \tag{38}$$

With the eigenvalue decomposition (EVD) of Eq. (38), we can obtain the noise subspace $\mathbf{E}_n$, and the two-dimensional MUSIC spectrum [2] is denoted as

$$P_{\text{2D - MUSIC}} = \frac{1}{\mathbf{c}^H(\theta,\varphi)\mathbf{E}_n\mathbf{E}_n^H\mathbf{c}(\theta,\varphi)} \tag{39}$$

where $\mathbf{c}(\theta,\varphi) = \overleftrightarrow{\mathbf{h}}(\theta,\varphi)$. Notice that Eq. (39) requires to search for both DOA and non-circular phases, which increases the complexity of the calculation. According to [45], [46], we introduce the expression for the reduced dimensional MUSIC (RD-MUSIC) method for the SD co-array. The directional vector $\mathbf{c}(\theta_k,\varphi_k)$ can be restructured as

$$\begin{aligned}\mathbf{c}(\theta_k,\varphi_k) &= \mathbf{C}(\theta_k)\boldsymbol{\nu}(\varphi_k)\\ &= \begin{bmatrix}\mathbf{c}_{S^-}(\theta_k) & \mathbf{0}_{M'\times 1} & \mathbf{0}_{M'\times 1}\\ \mathbf{0}_{(M_1+1)\times 1} & \mathbf{c}_D(\theta_k) & \mathbf{0}_{(M_1+1)\times 1}\\ \mathbf{0}_{M'\times 1} & \mathbf{0}_{M'\times 1} & \mathbf{c}_{S^+}(\theta_k)\end{bmatrix}\begin{bmatrix}e^{2j\varphi_k}\\ 1\\ e^{-2j\varphi_k}\end{bmatrix}\end{aligned} \tag{40}$$

with

$$\mathbf{c}_{S^-}(\theta_k) = \begin{bmatrix}e^{-j(M_1-M_2)\pi\sin\theta_k}\\ \vdots\\ 1\end{bmatrix} \tag{41}$$

$$\mathbf{c}_D(\theta_k) = \begin{bmatrix}1\\ e^{-j\pi\sin\theta_k}\\ \vdots\\ e^{-jM_1\pi\sin\theta_k}\end{bmatrix} \tag{42}$$

$$\mathbf{c}_{S^+}(\theta_k) = \begin{bmatrix}e^{-jM_1\pi\sin\theta_k}\\ e^{-j(M_1+1)\pi\sin\theta_k}\\ \vdots\\ e^{-jM_2\pi\sin\theta_k}\end{bmatrix} \tag{43}$$

where $M' = M_2 - M_1 + 1$, Let

$$\begin{aligned}\Theta(\theta,\varphi) &= \frac{1}{P_{\text{2D}-\text{MUSIC}}}\\ &= \mathbf{c}^H(\theta,\varphi)\mathbf{E}_n\mathbf{E}_n^H\mathbf{c}(\theta,\varphi)\\ &= \boldsymbol{\nu}^H(\varphi)\mathbf{C}^H(\theta)\mathbf{E}_n\mathbf{E}_n^H\mathbf{C}(\theta)\boldsymbol{\nu}(\varphi)\\ &= \boldsymbol{\nu}^H(\varphi)\mathbf{G}(\theta)\boldsymbol{\nu}(\varphi)\end{aligned} \tag{44}$$

where $\mathbf{G}(\theta) = \mathbf{C}^H(\theta)\mathbf{E}_n\mathbf{E}_n^H\mathbf{C}(\theta)$. Inspired by our previous work [45], the spectrum function of RD-MUSIC method can be written as

$$P_{\text{RD}-\text{MUSIC}} = \mathbf{e}^H\left(\mathbf{C}^H(\theta)\mathbf{E}_n\mathbf{E}_n^H\mathbf{C}(\theta)\right)^{-1}\mathbf{e} \tag{45}$$

where $\mathbf{e} = [0,1,0]^T$ such that $\mathbf{e}^H\boldsymbol{\nu}(\varphi) = 1$.

The main difference between the NA-NC-EBNC method and the NA-NC-BNC method is that the BNC matrix $\mathbf{R}^{\text{BNC}}$ is replaced by the EBNC matrix $\mathbf{R}^{\text{EBNC}}$. The specific processes of the two methods are given in Algorithm 1 and 2, respectively.

Algorithm 1 NA-NC-BNC DOA estimation method.

Input: $\mathbf{y}(t)$.
1: Calculate the BNC matrix $\mathbf{R}^{\text{BNC}}$ according to Eq. (20).
2: Vectorize and rearrange $\mathbf{R}^{\text{BNC}}$ by Eqs. (21)-(29), we can obtain: $\tilde{\mathbf{z}}_{\text{ULA}} = \mathbf{F}\tilde{\mathbf{z}} = [\tilde{\mathbf{z}}_1;\tilde{\mathbf{z}}_2;\tilde{\mathbf{z}}_3;\tilde{\mathbf{z}}_4]$, where $\tilde{\mathbf{z}} = \mathbf{J}\mathbf{z} = \tilde{\mathbf{H}}\mathbf{p} + \mathbf{J}vec(\mathbf{\Gamma})$ and $\mathbf{z} = vec\left(\mathbf{R}^{\text{BNC}}\right) = (\mathbf{B}^*\odot\mathbf{B})\,\mathbf{p} + vec(\mathbf{\Gamma})$.
3: Calculate the spatial smoothing matrix: $\mathbf{Z} = \left[\tilde{\mathbf{Z}}_{S^-};\tilde{\mathbf{Z}}_D;\tilde{\mathbf{Z}}_{S^+}\right] \in \mathbb{C}^{(2M_2-M_1+3)\times(M_1+1)}$, where $\tilde{\mathbf{Z}}_D$, $\tilde{\mathbf{Z}}_{S^-}$ and $\tilde{\mathbf{Z}}_{S^+}$ can be calculated by Eqs. (30)-(32).
4: Calculate the spatial smoothing covariance matrix $\mathbf{R}_Z$ of $\mathbf{Z}$: $\mathbf{R}_Z = \frac{1}{M_1+1}\mathbf{Z}\mathbf{Z}^H$.
5: By applying EVD to $\mathbf{R}_Z$, we can get the noise subspace $\mathbf{E}_n$.
6: Perform RD-MUSIC method with Eq. (45) for DOA estimation.

Algorithm 2 NA-NC-EBNC DOA estimation method.

Input: $\mathbf{y}(t)$.
1: Calculate the EBNC matrix $\mathbf{R}^{\text{EBNC}}$ according to Eq. (18).
2: Vectorize and rearrange the $\mathbf{R}^{\text{EBNC}}$ are similar to Algorithm 1.
3: Calculate the spatial smoothing matrix is similar to Eqs. (30)-(33).
4: Assuming that the spatial smoothing matrix constructed in step 3 can be expressed as $\mathbf{Z}'$, then the new covariance matrix $\mathbf{R}_{Z'}$ of the SD co-array: $\mathbf{R}_{Z'} = \frac{1}{M_1+1}\mathbf{Z}'\mathbf{Z}'^H$.
5: The remaining EVD and RD-MUSIC methods are the same as in Algorithm 1.

IV. Numerical Result

A. Evaluation and Measurement

The root mean square error (RMSE) can be defined as

$$\text{RMSE} = \sqrt{\frac{1}{\text{MC}}\sum_{j=1}^{\text{MC}}\frac{1}{K}\sum_{k=1}^{K}\left(\tilde{\theta}_{kj} - \theta_k\right)^2} \tag{46}$$

where $\tilde{\theta}_{kj}$ is the DOA estimate value at j-th Monte Carlo (MC) simulation. and the generalized signal to noise ratio (GSNR) [41] for non-circular signals can be expressed as:

$$\text{GSNR} = 10\log\left(\mathbb{E}\left\{|\mathbf{s}(t)|^2\right\}/\gamma\right) \tag{47}$$

TABLE I: Experimental conditions for Cases 1 to 3

Conditions	Case 1	Case 2	Case 3
α	1.5	0.5	$\alpha \in [0.1, 2]$
p	$p = 1.2$	$p = 0.9$	$p = 1.1$
$P = 9$	$N_1 = 4, N_2 = 5$	$N_1 = 4, N_2 = 5$	$N_1 = 4, N_2 = 5$

where $\mathbf{s}(t) = \mathbf{\Phi}\mathbf{s}_0(t)$ and γ is the dispersion parameter.

B. Complexity analysis

Throughout this section, the number of multiplications of real (or complex) values is considered as a complexity criterion. Calculate BNC and EBNC matrices costs $O\left\{\left(4P^2+8P\right)T\right\}$ and $O\left\{\left(4P^2+9P\right)T\right\}$, respectively. Compute the covariance matrix $\mathbf{R}_Z$ is $O\left\{M_0^2\left(M_1+1\right)\right\}$, and the eigenvalue decomposition (EVD) costs ${M_0}^3$, where $M_0 = 2M_2 - M_1 + 3$. The RD-MUSIC method needs a complexity of $O\left\{M_0^2\left(M_0-K\right)+n_s\left(3M_0^2+9M_0\right)\right\}$, where n_s is the search times. Then the total complexity of the proposed NA-NC-BNC algorithm is $O\{\left(4P^2+8P\right)T + M_0^2\left(M_1+1\right)+M_0^3+M_0^2\left(M_0-K\right)+n_s\left(3M_0^2+9M_0\right)\}$, and the proposed NA-NC-EBNC method with complexity of $O\{\left(4P^2+9P\right)T+M_0^2\left(M_1+1\right)+M_0^3+M_0^2\left(M_0-K\right)+n_s\left(3M_0^2+9M_0\right)\}$.

C. Selection of parameter p

In the proposed method, the EBNC matrix in Eq. (18) is used to replace the BNC matrix in Eq. (12), which involves the choice of parameter p. The value of p can be determined by experimental studies and the estimation performance is evaluated based on the RMSE with more than 1000 MC runs. The experimental results of the preliminary study for the case of different values of p are given in Fig. 3, where $\alpha = 0.5$ or $\alpha = 1.5$.

Cases 1 and 2 give detailed simulation results according to the different choices of parameter p. (Case 1 considers the algorithm performance in $\alpha = 1.5$ environment and Case 2 elaborates the scenario with $\alpha = 0.5$). It can be seen that the proposed NC-NA-EBNC method has a better estimation performance when p is set to 1.2 and 0.9 in Cases 1 and 2, respectively. Therefore, we take $p = 1.2$ in Case 1 and choose $p = 0.9$ in Case 2. It can also be observed that the estimation performance does not change significantly for $p \in [0.8, 1.2]$. In Cases 3, we analyse the performance of the algorithm for different values of impulsive characteristic exponent α when $p = 1.1$. The specific experimental conditions for the three cases are given in TABLE I.

D. Simulation results

We perform three simulations for discussing the RMSE performance of the proposed NC-NA-BNC and NC-NA-EBNC methods. We also give some simulation examples to demonstrate the performance of the various methods: the proposed methods, the PFLOM-MUSIC method [29], a correntropy-based covariance matrix MUSIC (CBCM-MUSIC) method [34], one correntropy-based correlation MUSIC (CRCO-MUSIC) method [30], an extended covariant non-circular

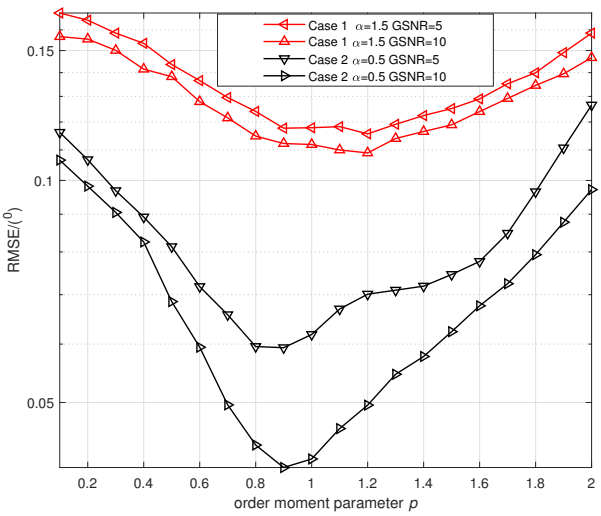

Fig. 3: RMSE versus parameter p, $T = 500$.

MUSIC method (EX-NC-MUSIC, [41]), a non-circular generalized covariance MUSIC (NC-GC-MUSIC) [47] method, a non-circular BNC MUSIC method (NC-BNC-MUSIC) [43], SBL [26] method and l_p-MUSIC method [27]. Also the Cramer-Rao Bound (CRB) in [26], [27] for impulsive noise is added for a comparison. However, for other α (except $\alpha = 1$ or $\alpha = 2$), the related PDF of impulsive noise hasn't closed-form expression. In this case, [47] states that linear interpolation can determine the coefficients between $\alpha = 1$ and $\alpha = 2$. Some key parameters of the above methods are given in TABLE II.

1) MUSIC spectrum for 1 MC: We first describe the MUSIC spectrum of a non-circular signal using nested or ULA with comparison methods EX-NC-MUSIC, NC-GC-MUSIC, NC-BNC-MUSIC, NC-NA-BNC and NC-NA-EBNC. The parameters of the experiment are: $N_1 = 3, N_2 = 4$, $T = 1000$, GSNR = 10 dB, $\alpha = 1.5$, the number of signals $K = 11$ and DOA = $-60°+12(k-1)(k = 1, 2, \cdots, K)$, non-circular phase $-30° + 6(k-1)(k = 1, 2, \cdots, K)$. From Figs. 4(d) and 4(e), the proposed NA-NC-BNC and NA-NC-EBNC algorithms can detect all 11 NC signals. As can be seen from Figs. 4(a)-4(c), for the ULA array, the NC characteristics also increase the number of detectable signals (the number of physical array elements is only 7). However, because of the impulsive noise interference, these five algorithms all eliminate the impulsive noise by proposing equivalent replaceable covariance matrices, where the proposed NA-NC-EBNC method results in spectral peaks closer to the real DOA. Furthermore, we compare the proposed NA-NC-EBNC method in Fig. 4 with the recently reported methods in cases 1-3.

*2) **Case** 1:* There are three incoherent sources impinging on the nested array with DOA $[0°, 10°, 20°]$ and non-circular phase $[10°, 20°, 30°]$. The impulsive noise characteristic exponent $\alpha = 1.5$, $p = 1.2$ and $N_1 = 4, N_2 = 5$.

Fig. 5(a) demonstrates the RMSE performance with different GSNR and the RMSE results versus the number of snapshots are illustrated in Fig. 5(b). It can be seen from

TABLE II: Parameter settings for different methods

Algorithms	Array structure and signal model	correlation theories	Mapping functions	parameter enactment
PFLOM-MUSIC [29]	ULA and circular signals	FLOS	PFLOM	$b = 0.05$
CBCM-MUSIC [34]	ULA and circular signals	Correntropy-based	Guassian function	$\mu = 0.7, \sigma = 10$
CRCO-MUSIC [30]	ULA and circular signals	Correntropy-based	Guassian function	$\sigma = 1.4\sigma_s, \mu = 0.5$
EXC-NC-MUSIC [41]	ULA and non-circular signals	FLOS	FLOM	$p = 1.2$
NC-GC-MUSIC [47]	ULA and non-circular signals	GC	Cauchy Score, Gaussian covariance	λs as in [47] and $\sigma^{\beta} = 10$
NC-BNC-MUSIC [43]	ULA and non-circular signals	BNC	Cauchy Score	$\lambda_3 = 0.4, \lambda_4 = 0.58$
l_p-MUSIC [27]	ULA and circular signals	Norm property	no	$p = 1.6$
SBL method [26]	ULA and circular signals	Sparse bayesian learning	no	the same as [26]
NC-NA-BNC	NA and non-circular signals	BNC	Cauchy Score	$\lambda_3 = 0.4, \lambda_4 = 0.58$
NC-NA-EBNC	NA and non-circular signals	proposed EBNC	Cauchy Score	$\lambda_3 = 0.4, \lambda_4 = 0.58$

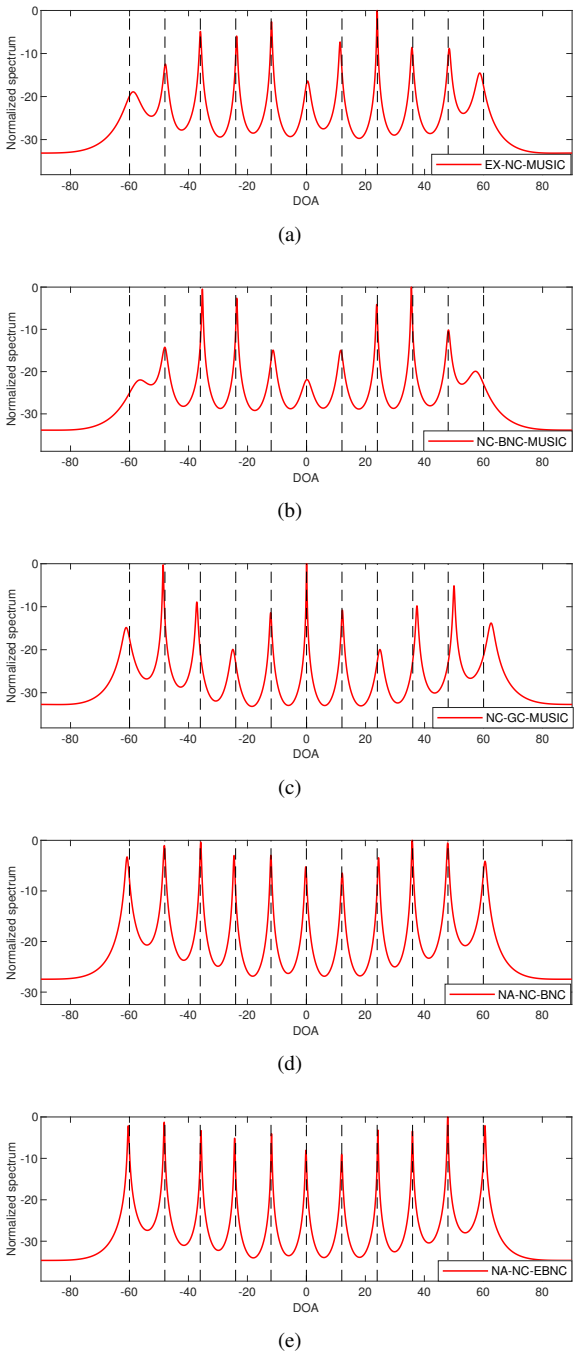

Fig. 4: Spectrum of the proposed NA-NC-BNC and NA-NC-EBNC methods, EX-NC-MUSIC method, NC-BNC-MUSIC method and NC-GC-MUSIC method, where $N_1 = 3, N_2 = 4$, $\alpha = 1.5$, $T = 1000$, GSNR = 10 dB, MC = 1. (a) EX-NC-MUSIC method; (b) NC-BNC-MUSIC method; (c) NC-GC-MUSIC method; (d)NA-NC-BNC method; (e) NA-NC-EBNC method.

Fig. 5(a) that the RMSE curves of PFLOM-MUSIC, CRCO-MUSIC, NC-BNC-MUSIC, EXC-NC-MUSIC and NC-GC-MUSIC methods become relatively flat when the GSNR is larger than 4 dB. The reason lies in their limited ability of combating the impulsive noise. In contrast, since the sparse array based methods can improve the estimation accuracy compared to the classical ULA, the two algorithms proposed in this paper are more robust in comparison. In addition, it can be seen from Fig. 5(a) that the estimation performance of the proposed two methods is better than the existing methods (iclude l_p-MUSIC and SBL methods) under the same GSNR condition. In addition, the performance of the l_p-MUSIC method performs poorly, but the SBL method shows good performance at GSNR > 0 dB. However, its performance is weaker than the NA-NC-BNC and NA-NC-EBNC methods because its grid is not off-grid. Compared with the proposed NA-NC-BNC method, the proposed NA-NC-EBNC method has better performance, which also indicates that EBNC matrix has stronger ability to fight against the impulsive interference than BNC matrix. Similar performance results can be observed in Fig. 5(b) , where the number of snapshots is variable.

*3) **Case** 2:* Since the l_p-MUSIC, CBCM-MUSIC, CRCO-MUSIC and EXC-NC-MUSIC methods only deal with $1 < \alpha < 2$, therefore, in this simulation, PFLOM-MUSIC method, NC-BNC-MUSIC method, NC-GC-MUSIC method, SBL method and the proposed two methods are considered for comparison.

Fig. 6(a) illustrates the RMSE performance for different GSNR scenarios and Fig. 6(b) shows the RMSE results for different number of snapshots. The results show that the performance of all five methods improves with the increase of GSNR and snapshots. Compared with the PFLOM-MUSIC method, NC-BNC-MUSIC method, SBL and NC-GC-MUSIC methods, the NA-based methods have better RMSE performance. However, the performance of the proposed NA-NC-BNC method is poor when GSNR < 1 dB, while the RMSE performance of the proposed NA-NC-EBNC method is always optimal, highlighting the ability of EBNC to combat the impulsive noise in highly impulsive scenarios ($0 < \alpha < 1$). The RMSE performance versus the number of snapshots shown in Fig. 6(b) also verifies the superiority of the proposed methods.

*4) **Case** 3:* The RMSE results in terms of characteristic exponent α ranges from 0.1 to 2 are provided in Fig. 7(a) and α from 0.1 to 1 is provided in Fig. 7(b), where MC = 1000, GSNR = 10 dB, $T = 500$. Other parameters are the same as case 1. It can be seen from Fig. 7(a), the

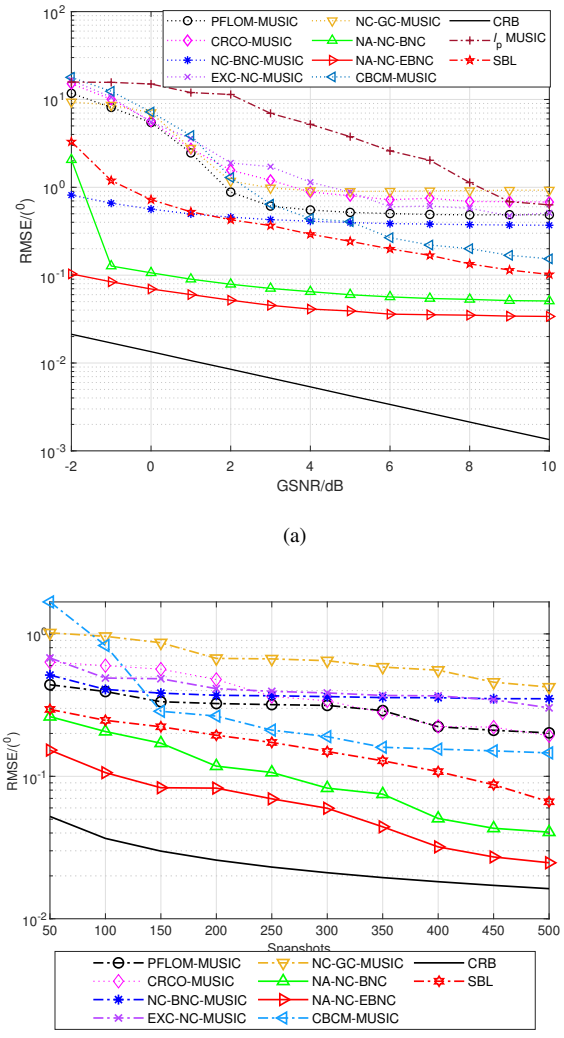

(a)

(b)

Fig. 5: RMSE of DOA estimation versus (a) GSNR, where $\alpha = 1.5$, $T = 500$, MC = 1000. (b) Snapshots, where $\alpha = 1.5$, GSNR = 10 dB, MC = 1000.

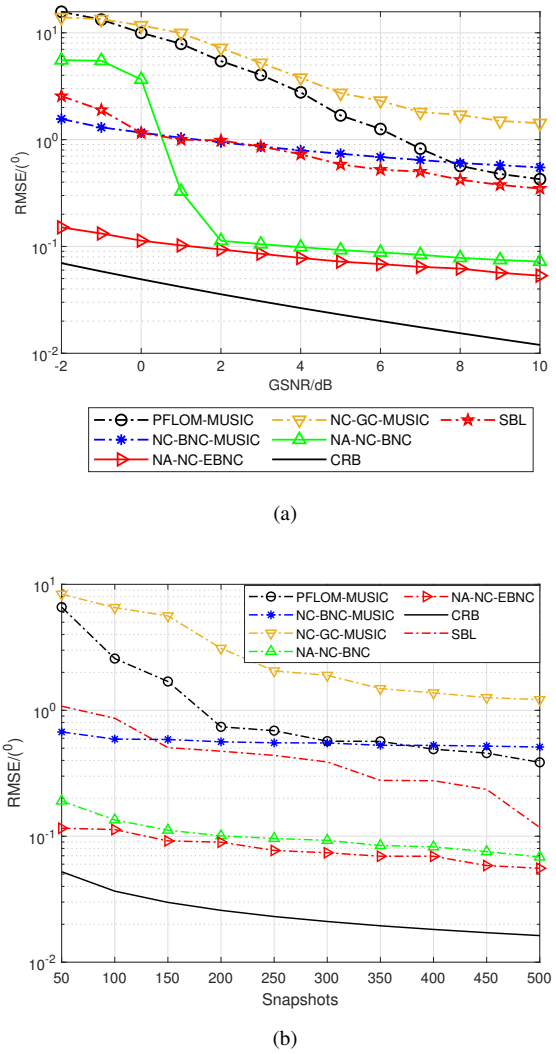

(a)

(b)

Fig. 6: RMSE of DOA estimation versus (a) GSNR, where $\alpha = 0.5$, $T = 500$, MC = 1000. (b) Snapshots, where $\alpha = 0.5$, GSNR = 10 dB, MC = 1000.

performance of these methods, except for the CBCM-MUSIC and EXC-NC-MUSIC algorithms, remains almost stable as the value of α increases continuously. Compared to other methods, the proposed NA-NC-EBNC method has the best RMSE performance. In addition, in highly impulsive scenario (shown in Fig. 7(b)), only the proposed method shows good performance. Comparing Fig. 7(a) and 7(b), it is found that the performance improvement of the proposed method in this paper is obvious in the highly impulsive environment, which also indicates that EBNC has a good ability to fight against the highly impulsive noise.

5) Comparison of ESPRIT and RD-MUSIC methods: In this section, the performance of RD-MUSIC is tested compared with the total least square ESPRIT (TLS-ESPRIT) [3] method when $0 < \alpha < 1$. The simulation parameters: two independent sources with DOA $[10°, 20°]$ and non-circular phase $[20°, 30°]$. $\alpha = 0.5$, $p = 1.2$ and $N_1 = 4, N_2 = 5$, $T = 500$, MC = 1000. Fig. 8 depicts the RMSE of the TLS-ESPRIT and RD-MUSIC methods for different GSNR scenarios. It is shown that the performance of both methods improves with the increase of GSNR. Compared with the BNC-based method, the EBNC-based method has a better estimation performance, highlighting the resistance to highly impulsive noise of the EBNC method. It can be found that although the TLS-ESPRIT method avoids the spectral peak search and reduces the computational complexity, its performance is still weaker than that of the RD-MUSIC method.

V. CONCLUSION

In this paper, we present an EBNC-based method, called NA-NC-EBNC, for DOA estimation of non-circular signals with nested arrays of impulsive noise. Moreover, the RD-MUSIC method is applied to DOA estimation to avoid the time-consuming two-dimensional search. Compared with the existing noise-resistance methods (such as CBCM-MUSIC, CRCO-MUSIC, EX-NC-MUSIC, NC-GC-MUSIC and NC-BNC-MUSIC methods), the proposed EBNC-based method is more robust to impulsive noise in DOA estimation. Simulations indicate that the proposed method provides better

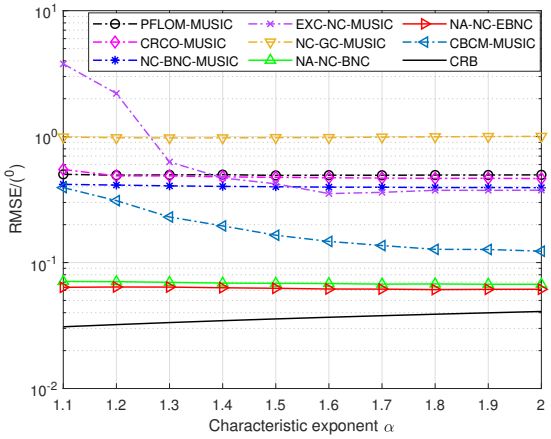

(a)

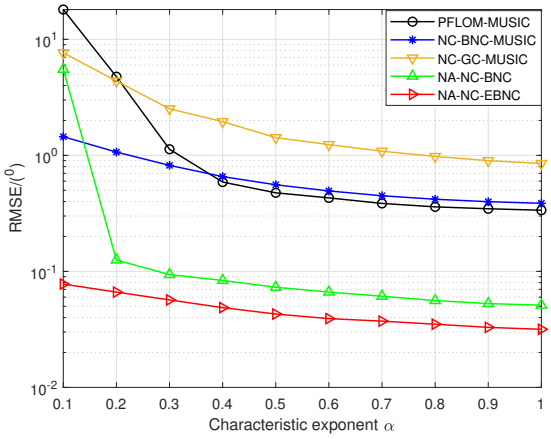

(b)

Fig. 7: RMSE performance (a) $\alpha \in \langle 1.1, 2\rangle$, (b) $\alpha \in \langle 0.1, 1\rangle$.

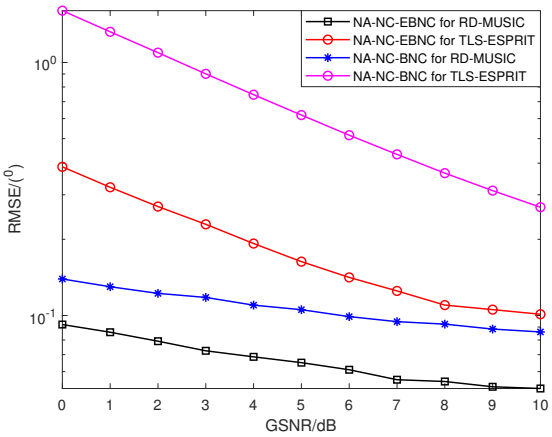

Fig. 8: RMSE versus GSNRs, $\alpha = 0.5$, and $T = 500$, MC = 1000.

performance in the case of impulsive noise, especially at low GSNRs and smaller parameter α.

APPENDIX

A. Proof of Eq. (14)

Firstly, we analyse the sub-matrix $\mathbf{R}^1_{\mathrm{BNC}}$. In order to accurately extract DOAs from the received signal, the intensity of impulsive noise interference needs to be reduced. The BNC function can effectively combat the highly impulsive noise interference and the BNC function is almost linear. According to Eq. (2) and Eq. (11), the (i,j) element of $\mathbf{R}^1_{\mathrm{BNC}}$ is

$$\begin{aligned} r^1_{ij} &= \mathrm{BNC}\left(\mathbf{x}_i(t), \mathbf{x}_j(t)\right) \\ &= \mathrm{BNC}\left[\mathbf{A}_i\mathbf{s}(t) + n_i(t), \mathbf{A}_j\mathbf{s}(t) + n_j(t)\right] \\ &= \mathbb{E}\left\{g\left(\mathbf{A}_i\mathbf{s}(t) + n_i(t)\right) g^H\left(\mathbf{A}_j\mathbf{s}(t) + n_j(t)\right)\right\} \end{aligned} \tag{48}$$

Since the uncorrelated properties of the sources and the noise. From [43], Eq. (48) can be rewritten as

$$\begin{aligned} r^1_{ij} &= \mathbb{E}\left\{g\left(\mathbf{A}_i\mathbf{s}(t) + n_i(t)\right) g^H\left(\mathbf{A}_j\mathbf{s}(t) + n_j(t)\right)\right\} \\ &= \mathbb{E}\left\{g\left(\mathbf{A}_i\mathbf{s}(t)\right) g^H\left(\mathbf{A}_j\mathbf{s}(t)\right)\right\} + \mathbb{E}\left\{g\left(n_i(t)\right) g^H\left(n_j(t)\right)\right\} \\ &= \mathrm{BNC}\left[\mathbf{A}_i\mathbf{s}(t), \mathbf{A}_j\mathbf{s}(t)\right] + \mathbb{E}\left\{g\left(n_i(t)\right) g^H\left(n_j(t)\right)\right\} \\ &= \mathrm{BNC}\left[\mathbf{A}_i\mathbf{s}(t), \mathbf{A}_j\mathbf{s}(t)\right] + \sigma_n^2\delta_{ij} \end{aligned} \tag{49}$$

where σ_n^2 is the approximate variance of impulsive noise (according to [24], its exact form cannot be given, σ_n^2 can be seen as an approximation of the dispersion parameter γ) and δ_{ij} is the Kronecker delta function.

By the independence property of BNC (see [42] for a specific proof), we can obtain

$$\begin{aligned} &\mathrm{BNC}\left[\mathbf{A}_i\mathbf{s}(t), \mathbf{A}_j\mathbf{s}(t)\right] \\ &= \mathrm{BNC}\left[\sum_{k=1}^{K}\mathbf{a}_i(\theta_k) e^{-j\varphi_k} s_{0k}(t), \sum_{p=1}^{K}\mathbf{a}_j(\theta_p) e^{-j\varphi_p} s_{0p}(t)\right] \\ &= \sum_{k=1}^{K}\mathbf{a}_i(\theta_k) e^{-j\varphi_k}\mathrm{BNC}\left(s_{0k}(t), s_{0k}(t)\right)\left(\mathbf{a}_i(\theta_k) e^{-j\varphi_k}\right)^H \\ &= \sum_{k=1}^{K}\mathbf{a}_i(\theta_k) e^{-j\varphi_k}\mathrm{BNC}\left(s_{0k}(t), s_{0k}(t)\right) e^{j\varphi_k}\mathbf{a}_i^*(\theta_k) \\ &= \mathbf{A}_i\mathbf{\Phi}\mathbf{R}^{\mathrm{BNC}}_{s_0}\mathbf{\Phi}^H\mathbf{A}_j^H \end{aligned} \tag{50}$$

where $\mathbf{R}^{\mathrm{BNC}}_{\mathbf{s}0} = diag\left(\kappa_{01}, \cdots, \kappa_{0k}, \cdots, \kappa_{0K}\right)$ and $\kappa_{0k} = \mathrm{BNC}\left[s_{0k}(t), s_{0k}(t)\right]$. Then (48) can be expressed as

$$r^1_{ij} = \mathbf{A}_i\mathbf{\Phi}\mathbf{R}^{\mathrm{BNC}}_{s_0}\mathbf{\Phi}^H\mathbf{A}_j^H + \sigma_n^2\delta_{ij} \tag{51}$$

In the same way, we have

$$r^2_{ij} = \mathbf{A}_i\mathbf{\Phi}\mathbf{R}^{\mathrm{BNC}}_{\mathbf{s}0}\mathbf{\Phi}^T\mathbf{A}_j^T \tag{52}$$

$$r^3_{ij} = \mathbf{A}_i^*\mathbf{\Phi}^*\mathbf{R}^{\mathrm{BNC}}_{\mathbf{s}0}\mathbf{\Phi}^H\mathbf{A}_j^H \tag{53}$$

$$r^4_{ij} = \mathbf{A}_i^*\mathbf{\Phi}^*\mathbf{R}^{\mathrm{BNC}}_{\mathbf{s}0}\mathbf{\Phi}^T\mathbf{A}_j^T + \sigma_n^2\delta_{ij} \tag{54}$$

According to Eq. (49), we obtain

$$\begin{aligned}
&\mathbf{R}_{\mathrm{BNC}}^{1} \\
&= \begin{bmatrix} \mathbf{A}_1\mathbf{\Phi}\mathbf{R}_{\mathbf{s}0}^{\mathrm{BNC}}\mathbf{\Phi}^H\mathbf{A}_1^H & \cdots & \mathbf{A}_1\mathbf{\Phi}\mathbf{R}_{\mathbf{s}0}^{\mathrm{BNC}}\mathbf{\Phi}^H\mathbf{A}_P^H \\ \vdots & \ddots & \vdots \\ \mathbf{A}_P\mathbf{\Phi}\mathbf{R}_{\mathbf{s}0}^{\mathrm{BNC}}\mathbf{\Phi}^H\mathbf{A}_1^H & \cdots & \mathbf{A}_P\mathbf{\Phi}\mathbf{R}_{\mathbf{s}0}^{\mathrm{BNC}}\mathbf{\Phi}^H\mathbf{A}_P^H \end{bmatrix} + \sigma_n^2\mathbf{I}_P \\
&= \begin{bmatrix} \mathbf{A}_1 \\ \vdots \\ \mathbf{A}_P \end{bmatrix} \mathbf{\Phi}\mathbf{R}_{\mathbf{s}0}^{\mathrm{BNC}}\mathbf{\Phi}^H \begin{bmatrix} \mathbf{A}_1^H, & \cdots, & \mathbf{A}_P^H \end{bmatrix} + \sigma_n^2\mathbf{I}_P \\
&= \mathbf{A}\mathbf{\Phi}\mathbf{R}_{\mathbf{s}0}^{\mathrm{BNC}}\mathbf{\Phi}^H\mathbf{A}^H + \sigma_n^2\mathbf{I}_P
\end{aligned} \tag{55}$$

Similarly,

$$\mathbf{R}_{\mathrm{BNC}}^{2} = \mathbf{A}\mathbf{\Phi}\mathbf{R}_{\mathbf{s}0}^{\mathrm{BNC}}\mathbf{\Phi}^T\mathbf{A}^T \tag{56}$$

$$\mathbf{R}_{\mathrm{BNC}}^{3} = \mathbf{A}^*\mathbf{\Phi}^*\mathbf{R}_{\mathbf{s}0}^{\mathrm{BNC}}\mathbf{\Phi}^H\mathbf{A}^H \tag{57}$$

$$\mathbf{R}_{\mathrm{BNC}}^{4} = \mathbf{A}^*\mathbf{\Phi}^*\mathbf{R}_{\mathbf{s}0}^{\mathrm{BNC}}\mathbf{\Phi}^T\mathbf{A}^T + \sigma_n^2\mathbf{I}_P \tag{58}$$

Then, Eq. (12) can be rewritten as

$$\begin{aligned}
&\mathbf{R}^{\mathrm{BNC}} = \mathrm{BNC}\left(\mathbf{X}\left(t\right), \mathbf{X}\left(t\right)\right) = \begin{bmatrix} \mathbf{R}_{\mathrm{BNC}}^{1} & \mathbf{R}_{\mathrm{BNC}}^{2} \\ \mathbf{R}_{\mathrm{BNC}}^{3} & \mathbf{R}_{\mathrm{BNC}}^{4} \end{bmatrix} \\
&= \begin{bmatrix} \mathbf{A}\mathbf{\Phi}\mathbf{R}_{\mathbf{s}0}^{\mathrm{BNC}}\mathbf{\Phi}^H\mathbf{A}^H & \mathbf{A}\mathbf{\Phi}\mathbf{R}_{\mathbf{s}0}^{\mathrm{BNC}}\mathbf{\Phi}^T\mathbf{A}^T \\ \mathbf{A}^*\mathbf{\Phi}^*\mathbf{R}_{\mathbf{s}0}^{\mathrm{BNC}}\mathbf{\Phi}^H\mathbf{A}^H & \mathbf{A}^*\mathbf{\Phi}^*\mathbf{R}_{\mathbf{s}0}^{\mathrm{BNC}}\mathbf{\Phi}^T\mathbf{A}^T \end{bmatrix} + \sigma_n^2\mathbf{I}_{2P} \\
&= \begin{bmatrix} \mathbf{A}\mathbf{\Phi} \\ \mathbf{A}^*\mathbf{\Phi}^* \end{bmatrix} \mathbf{R}_{\mathbf{s}0}^{\mathrm{BNC}} \left[\mathbf{\Phi}^H\mathbf{A}^H, \mathbf{\Phi}^T\mathbf{A}^T\right] + \mathbf{\Gamma} \\
&= \hat{\mathbf{A}}R_{\mathbf{s}0}^{\mathrm{BNC}}\hat{\mathbf{A}}^H + \mathbf{\Gamma}
\end{aligned} \tag{59}$$

where $\hat{\mathbf{A}} = [\mathbf{A}\mathbf{\Phi}; \mathbf{A}^*\mathbf{\Phi}^*]$ and $\mathbf{\Gamma} = \sigma_n^2\mathbf{I}_{2P}$ is a scalar matrix, thus we have $\mathbf{R}^{\mathrm{BNC}}$ shown in (14).

Remark 4: The proof of r_{ij}^1 in [43] eliminates the non-circular phase $\mathbf{\Phi}$, and it considers (50) as follows

$$\begin{aligned}
&\mathrm{BNC}\left[\mathbf{A}_i\mathbf{s}\left(t\right), \mathbf{A}_j\mathbf{s}\left(t\right)\right] \\
&= \sum_{k=1}^{K} \mathbf{a}_i\left(\theta_k\right) e^{-j\varphi_k} \mathrm{BNC}\left(s_{0k}\left(t\right), s_{0k}\left(t\right)\right) \left(\mathbf{a}_i\left(\theta_k\right) e^{-j\varphi_k}\right)^H \\
&= \sum_{k=1}^{K} \mathbf{a}_i\left(\theta_k\right) e^{-j\varphi_k} \mathrm{BNC}\left(s_{0k}\left(t\right), s_{0k}\left(t\right)\right) e^{j\varphi_k} \mathbf{a}_i^*\left(\theta_k\right) \\
&= \sum_{k=1}^{K} \mathbf{a}_i\left(\theta_k\right) e^{-j\varphi_k} e^{j\varphi_k} \mathbf{a}_i^*\left(\theta_k\right) \mathrm{BNC}\left(s_{0k}\left(t\right), s_{0k}\left(t\right)\right) \\
&= \sum_{k=1}^{K} \mathbf{a}_i\left(\theta_k\right) \mathbf{a}_i^*\left(\theta_k\right) \mathrm{BNC}\left(s_{0k}\left(t\right), s_{0k}\left(t\right)\right)
\end{aligned} \tag{60}$$

Thus, it obtains the result of

$$\mathbf{R}^{\mathrm{BNC}} = \begin{bmatrix} \mathbf{A} \\ \mathbf{A}^*\mathbf{\Phi}^* \end{bmatrix} \mathbf{R}_{\mathbf{s}0}^{\mathrm{BNC}} \begin{bmatrix} \mathbf{A} \\ \mathbf{A}^*\mathbf{\Phi}^* \end{bmatrix}^H + \mathbf{\Gamma} \tag{61}$$

From Eq. (8), it can be seen that the above covariance matrix (61) loses the phase information, which is in contradiction with the extended directional matrix $\mathbf{B}$. Therefore, the non-circular phase in (50) cannot be eliminated.

B. Boundedness proof of Eq. (15)

In Eq. (13), we have

$$\begin{aligned}
&\exists f_0 > 0, \text{s.t. } \max\left|f\left(x\right)\right| \leqslant f_0 \\
&\forall x \in \mathbb{R}/\left(-x_0, x_0\right)
\end{aligned} \tag{62}$$

i.e., $g(x)$ is bounded, and then we prove $G(x)$ is also bounded.

Generally, the impulsive disturbance values are particularly large, so we consider $x_0 \gg 1$. Then when $x \geqslant x_0$, we have

$$\exists x' > x_0 \gg 1, \text{s.t.} f\left(x'\right) = f_0 \tag{63}$$

According to Eq. (15), we can obtain

$$\left|x'\right|^{p-2}x' \leqslant x', 0 < p \leqslant 2 \tag{64}$$

where $\left|x'\right|^{p-2} \leqslant 1$. According to (63), then

$$f\left(\left|x'\right|^{p-2}x'\right) \leqslant f\left(x'\right) = f_0, \forall x \geqslant x_0 \tag{65}$$

Similarly, when $x \leqslant -x_0$ we have $f\left(\left|x\right|^{p-2}x\right) \geqslant -f_0$. So that $\max\left|f\left(\left|x\right|^{p-2}x\right)\right| \leqslant f_0$, and $l\left(\left|x\right|^{p-2}x\right) \approx \left|x\right|^{p-2}x < x_0$, so $G(x)$ is bounded.

C. Convergence of r^{EBNC}

Property: According to [43], if X is a real stochastic variable and it obeys $S\alpha S$ distribution, its BNC matrix r^{BNC} converges.

Similarly, we assume that the probability density function of stochastic variable X can be expressed as $h_X(x)$, then $\mathbf{r}^{\mathrm{EBNC}}$ satisfies

$$\begin{aligned}
&r^{\mathrm{EBNC}}\left(X, X\right) = \mathbb{E}\left\{G\left(X\right)G^H\left(X\right)\right\} \\
&= \int \left|G\left(x\right)\right|^2 h_X\left(x\right)dx \leqslant \int f_0^2 h_X\left(x\right)dx = f_0^2
\end{aligned}$$

Therefore, in this case, it can be concluded that r^{EBNC} converges.

REFERENCES

[1] H. Krim and M. Viberg, "Two decades of array signal processing research: the parametric approach," *IEEE signal processing magazine*, vol. 13, no. 4, pp. 67–94, 1996.

[2] R. Schmidt, "Multiple emitter location and signal parameter estimation," *IEEE Transactions on Antennas and Propagation*, vol. 34, no. 3, pp. 276–280, 1986.

[3] R. Roy and T. Kailath, "ESPRIT-estimation of signal parameters via rotational invariance techniques," *IEEE Transactions on Acoustics, Speech and Signal Processing*, vol. 37, no. 7, pp. 984–995, 1989.

[4] A. Moffet, "Minimum-redundancy linear arrays," *IEEE Transactions on Antennas and Propagation*, vol. 16, no. 2, pp. 172–175, 1968.

[5] P. P. Vaidyanathan and P. Pal, "Sparse sensing with co-prime samplers and arrays," *IEEE Transactions on Signal Processing*, vol. 59, no. 2, pp. 573–586, 2011.

[6] W. Zheng, X. Zhang, Y. Wang, M. Zhou, and Q. Wu, "Extended coprime array configuration generating large-scale antenna co-array in massive MIMO system," *IEEE Transactions on Vehicular Technology*, vol. 68, no. 8, pp. 7841–7853, 2019.

[7] S. Qin, Y. D. Zhang, and M. G. Amin, "Generalized coprime array configurations for direction-of-arrival estimation," *IEEE Transactions on Signal Processing*, vol. 63, no. 6, pp. 1377–1390, 2015.

[8] C. Zhou, Y. Gu, X. Fan, Z. Shi, G. Mao, and Y. D. Zhang, "Direction-of-arrival estimation for coprime array via virtual array interpolation," *IEEE Transactions on Signal Processing*, vol. 66, no. 22, pp. 5956–5971, 2018.

[9] P. Pal and P. P. Vaidyanathan, "Nested arrays: A novel approach to array processing with enhanced degrees of freedom," *IEEE Transactions on Signal Processing*, vol. 58, no. 8, pp. 4167–4181, 2010.
[10] C. L. Liu and P. P. Vaidyanathan, "Super nested arrays: Linear sparse arrays with reduced mutual coupling part i: Fundamentals," *IEEE Transactions on Signal Processing*, vol. 64, no. 15, pp. 3997–4012, 2016.
[11] C. L. Liu and P. P. Vaidyanathan, "Super nested arrays: Linear sparse arrays with reduced mutual coupling part ii: High-order extensions," *IEEE Transactions on Signal Processing*, vol. 64, no. 16, pp. 4203–4217, 2016.
[12] J. Liu, Y. Zhang, Y. Lu, S. Ren, and S. Cao, "Augmented nested arrays with enhanced DOF and reduced mutual coupling," *IEEE Transactions on Signal Processing*, vol. 65, no. 21, pp. 5549–5563, 2017.
[13] J. P. Delmas and H. Abeida, "Cramer Rao bounds of DOA estimates for BPSK and QPSK modulated signals," *IEEE Transactions on Signal Processing*, vol. 54, no. 1, pp. 117–126, 2006.
[14] Z. M. Liu, Z. T. Huang, Y. Y. Zhou, and J. Liu, "Direction-of-arrival estimation of noncircular signals via sparse representation," *IEEE Transactions on Aerospace and Electronic Systems*, vol. 48, no. 3, pp. 2690–2698, 2012.
[15] J. Steinwandt, F. Roemer, M. Haardt, and G. D. Galdo, "Deterministic Cramer-Rao bound for strictly non-circular sources and analytical analysis of the achievable gains," *IEEE Transactions on Signal Processing*, vol. 64, no. 17, pp. 4417–4431, 2015.
[16] P. Gupta and M. Agrawal, "Design and analysis of the sparse array for DOA estimation of noncircular signals," *IEEE Transactions on Signal Processing*, vol. 67, no. 2, pp. 460–473, 2019.
[17] H. Abeida and J. Delmas, "MUSIC-like estimation of direction of arrival for noncircular sources," *IEEE Transactions on Signal Processing*, vol. 54, pp. 2678–2690, Jul. 2006.
[18] Y. Shi, L. Huang, C. Qian, and H. C. So, "Direction-of-arrival estimation for noncircular sources via structured least squares based ESPRIT using three-axis crossed array," *IEEE Transactions on Aerospace and Electronic Systems*, vol. 51, no. 2, pp. 1267–1278, 2015.
[19] Z. Chen, Y. Ding, S. Ren, and Z. Chen, "A novel noncircular MUSIC algorithm based on the concept of the difference and sum coarray," *Sensors*, vol. 18, no. 2, p. 344, 2018.
[20] P. Gupta and M. Agrawal, "Design and analysis of the sparse array for DOA estimation of noncircular signals," *IEEE Transactions on Signal Processing*, vol. 67, no. 2, pp. 460–473, 2019.
[21] Y. Wang, J. Shen, X. Zhang, Y. He, and X. Dai, "Noncircular signals for nested array: Sum-difference co-array and DOA estimation algorithm," *IET Radar Sonar and Navigation*, vol. 14, no. 4, 2019.
[22] Y. Wang, W. Wu, X. Zhang, and W. Zheng, "Transformed nested array designed for DOA estimation of non-circular signals: Reduced sum-difference co-array redundancy perspective," *IEEE Communications Letters*, vol. 24, no. 6, pp. 1262–1265, 2020.
[23] X. Zhang, Z. Zheng, W.-Q. Wang, and H. C. So, "DOA estimation of mixed circular and noncircular sources using nonuniform linear array," *IEEE Transactions on Aerospace and Electronic Systems*, vol. 58, no. 6, pp. 5703–5710, 2022.
[24] M. Shao and C. L. Nikias, "Signal processing with fractional lower order moments: stable processes and their applications," *Proceedings of the IEEE*, vol. 81, no. 7, pp. 986–1010, 1993.
[25] H. Huang, H. C. So, and A. M. Zoubir, "Extended cyclic coordinate descent for robust row-sparse signal reconstruction in the presence of outliers," in *ICASSP 2020-2020 IEEE International Conference on Acoustics, Speech and Signal Processing (ICASSP)*, pp. 4791–4795, IEEE, 2020.
[26] J. Dai and H. C. So, "Sparse Bayesian learning approach for outlier-resistant direction-of-arrival estimation," *IEEE Transactions on Signal Processing*, vol. 66, no. 3, pp. 744–756, 2017.
[27] W. Zeng, H. C. So, and L. Huang, "ℓ_p-MUSIC: Robust direction-of-arrival estimator for impulsive noise environments," *IEEE Transactions on Signal Processing*, vol. 61, no. 17, pp. 4296–4308, 2013.
[28] A. Mahmood, M. Chitre, and M. A. Armand, "PSK communication with passband additive symmetric α-stable noise," *IEEE Transactions on Communications*, vol. 60, no. 10, pp. 2990–3000, 2012.
[29] H. Belkacemi and S. Marco, "Robust subspace-based algorithms for joint angle/doppler estimation in non-gaussian clutter," *Signal Processing*, vol. 87, pp. 1547–1558, 2007.
[30] J. Zhang, T. Qiu, A. Song, and H. Tang, "A novel correntropy based DOA estimation algorithm in impulsive noise environments," *Signal Processing*, vol. 104, pp. 346–357, 2014.
[31] Q. Tian, T. Qiu, M. A. Jitong, L. I. Jingchun, and L. I. Rong, "Robust fractional lower order correntropy algorithm for DOA estimation in impulsive noise environments," *IEICE Transactions on Communications*, vol. E104.B, no. 1, 2020.
[32] F. Ma, H. Bai, X. Zhang, C. Xu, and Y. Li, "Generalised maximum complex correntropy-based DOA estimation in presence of impulsive noise," *IET Radar, Sonar and Navigation*, vol. 14, no. 6, pp. 793–802, 2020.
[33] P. Wang, T. Qiu, F. Ren, and A. Song, "A robust DOA estimator based on the correntropy in alpha-stable noise environments," *Digital Signal Processing*, vol. 60, pp. 242–251, 2017.
[34] J. Chen and S. Guan, "Correntropy-based DOA estimation algorithm under impulsive noise environments," *EURASIP Journal on Wireless Communications and Networking*, vol. 2020, no. 1, 2020.
[35] Z. M. Liu, Z.-T. Huang, and Y. Y. Zhou, "Array signal processing via sparsity-inducing representation of the array covariance matrix," *IEEE Transactions on Aerospace and Electronic Systems*, vol. 49, no. 3, pp. 1710–1724, 2013.
[36] Q. Liu, C. Yang, Y. Gu, and S. H. Cheung, "Robust sparse recovery via weakly convex optimization in impulsive noise," *Signal Processing*, vol. 152, pp. 84–89, 2018.
[37] Q. Liu, H. C. So, and Y. Gu, "Off-grid DOA estimation with nonconvex regularization via joint sparse representation," *Signal Processing*, vol. 140, pp. 171–176, 2017.
[38] Q. Liu, Y. Gu, and H. C. So, "Smoothed sparse recovery via locally competitive algorithm and forward euler discretization method," *Signal Processing*, vol. 157, pp. 97–102, 2019.
[39] R. Zheng, X. Xu, Z. Ye, and J. Dai, "Robust sparse Bayesian learning for DOA estimation in impulsive noise environments," *Signal Processing*, vol. 171, p. 107500, 2020.
[40] J. Zhang, T. Qiu, and S. Luan, "An efficient real-valued sparse Bayesian learning for non-circular signal's DOA estimation in the presence of impulsive noise," *Digital Signal Processing*, vol. 106, p. 102838, 2020.
[41] J. Zhang and T. Qiu, "A novel covariation based noncircular sources direction finding method under impulsive noise environments," *Signal Processing*, vol. 98, no. 5, pp. 252–262, 2014.
[42] S. Luan, T. Qiu, L. Yu, J. Zhang, A. Song, and Y. Zhu, "BNC-based projection approximation subspace tracking under impulsive noise," *IET Radar, Sonar and Navigation*, vol. 11, no. 7, pp. 1055–1061, 2017.
[43] J. Zhang, T. Qiu, S. Luan, and H. Li, "Bounded non-linear covariance based ESPRIT method for noncircular signals in presence of impulsive noise," *Digital Signal Processing*, vol. 87, pp. 104–111, 2019.
[44] X. Dong, M. Sun, X. Zhang, and J. Zhao, "Fractional low-order moments based DOA estimation with co-prime array in presence of impulsive noise," *IEEE Access*, vol. 9, pp. 23537–23543, 2021.
[45] X. Dong, X. Zhang, J. Zhao, and M. Sun, "Non-circular sources DOA estimation for coprime array with impulsive noise: A novel augmented phased fractional low-order moment," *IEEE Transactions on Vehicular Technology*, vol. 71, no. 10, pp. 10559–10569, 2022.
[46] X. Zhang, L. Xu, L. Xu, and D. Xu, "Direction of departure (DOD) and direction of arrival (doa) estimation in mimo radar with reduced-dimension music," *IEEE Communications Letters*, vol. 14, no. 12, pp. 1161–1163, 2010.
[47] S. Luan, J. Li, Y. Gao, J. Zhang, and T. Qiu, "Generalized covariance-based ESPRIT-like solution to direction of arrival estimation for strictly non-circular signals under α-stable distributed noise," *Digital Signal Processing*, vol. 118, p. 103214, 2021.

Xudong Dong received the M.S. degree in applied mathematics from Guilin University of Electronic Technology in 2020. He is pursuing the Ph.D. degree in communication and information systems with the College of Electronic and Information Engineering, Nanjing University of Aeronautics and Astronautics, Nanjing, China. His research interests are target detection and tracking, array signal processing, deep learning, signal classification and impulsive noise.

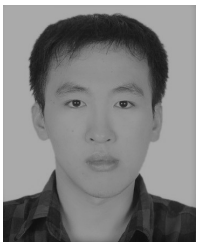

Meng Sun received his B.S. and his M.S. degrees from Northwest University and South China University of Technology, China in 2010 and 2013, respectively. He received the Ph.D. degree from IETR Laboratory at Polytech Nantes (Université de Nantes, France) in 2016. He is currently with Electronic Engineering Department, Nanjing University of Aeronautics and Astronautics, Nanjing, China. His main research focus on array signal processing, spectral analysis, and ground penetrating radar.

Jun Zhao received the M.S. degree in applied mathematics from the Guilin University of Electronic Technology, Guilin, China, in 2020. She is currently working toward the Ph.D. degree in information and communication engineering with the College of Electronic and Information Engineering, Tongji University, Shanghai, China. Her research interests include target detection and tracking, array signal processing, and machine learning.

Xiaofei Zhang received M.S degree from Wuhan University, Wuhan, China, in 2001. He received Ph.D. degrees in communication and information systems from Nanjing University of Aeronautics and Astronautics in 2005. Now, he is a Professor in Electronic Engineering Department, Nanjing University of aeronautics and astronautics, Nanjing, China. His research is focused on array signal processing and communication signal processing.

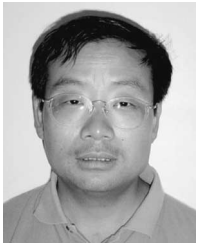

Yide Wang received the B.S. degree in electrical engineering from the Beijing University of Post and Telecommunication, Beijing, China, in 1985, and the M.S. and the Ph.D. degrees in signal processing and telecommunications from the University of Rennes, France, in 1986 and 1989, respectively. He is currently a Professor with the Ecole Polytechnique de l'Université de Nantes. His research interests include array signal processing, spectral analysis, and mobile wireless communication systems.